

The Distribution of Reduced Sulphur Compounds in Polar Environments:

Insights from Observations and Climatologies

by

Tereza Jarníková

B.Sc. McGill University 2012, Mathematics and Biology

A THESIS SUBMITTED IN PARTIAL FULFILLMENT OF

THE REQUIREMENTS FOR THE DEGREE OF

MASTER OF SCIENCE

in

THE FACULTY OF GRADUATE AND POSTDOCTORAL STUDIES

(Oceanography)

THE UNIVERSITY OF BRITISH COLUMBIA

(Vancouver)

April 2016

© Tereza Jarníková, 2016

Abstract

Dimethylsulfide (DMS) and dimethylsulfoniopropionate (DMSP) are key components in the marine reduced sulphur cycle, where they play several roles in the ecology of bacteria and phytoplankton. Upon emission to the atmosphere, DMS plays a role in atmospheric sulphur budgets and radiative balance, having potentially climate-cooling effects. This thesis aims to provide insight into the distribution of these compounds in polar marine waters. This is done by constructing a revised climatology of DMS budgets in the Southern Ocean and by presenting new DMS/P data in the Arctic Ocean.

Chapter 2 presents a revised summertime climatology of DMS distributions and fluxes in the Southern Ocean, based on the inclusion of a significant number of high-resolution measurements (~700 000) made in recent years. Based on the climatology written by Lana et al in 2011, the revised climatology shows notable differences in DMS budgets. In particular, we find increased DMS concentrations and sea–air fluxes south of the Polar Frontal zone (between 60 and 70°S), and increased sea–air fluxes in mid-latitude waters (40–50°S). These changes are attributable to both the inclusion of new data and the use of region-specific parameters (e.g. data cut-off thresholds and interpolation radius) in our objective analysis. DMS concentrations in the Southern Ocean exhibit weak though statistically significant correlations with several oceanographic variables, including ice cover, mixed-layer depth and chlorophyll-a.

Chapter 3 presents new DMS and DMSP measurements made in the Canadian sector of the Arctic Ocean on the 2015 GEOTRACES expedition, as well as estimates of sea-air fluxes and hydrographic data that presents some potential explanations for these distributions. Across the full sampling transect, we find weak relationships between DMSP:chl *a* ratios and known diatom marker pigments and elevated DMS/P in partially ice-covered areas. Our high spatial

resolution measurements allowed us to examine DMS variability over small scales, and to document DMS concentration gradients across surface hydrographic frontal features.

Together, these two chapters help to fill out the understanding of the distribution and cycling of reduced sulphur in polar marine waters, and can serve to provide a baseline for future reduced sulphur work in these regions.

Preface

The research contained in this thesis was carried out using instrumentation provided by the Tortell laboratory at the University of British Columbia. The data used to construct the climatology presented in Chapter 2 was collected using the MIMS system (developed by Tortell 2005), operated on several Antarctic expeditions by Chris Payne, Laughlin Barker, Casey Smith, and Constance Couture. Dr. Tortell initiated the construction of the climatology and provided the conceptual framework and motivation. I wrote the MATLAB code used to construct the climatology, adapting code previously written by Arancha Lana at CSIS. Chapter 2 has been accepted for publication in the journal *Environmental Chemistry* in 2015.

The data presented in Chapter 3 were collected using the MIMS and OSSCAR systems. OSSCAR was developed by Asher, Tortell, and Dacey in 2013-2015, and I made coding and hardware modifications to it and operated it during the 2015 GEOTRACES expedition to the Canadian Arctic. The MIMS system was operated by Dr. Tortell at that same time. I wrote the manuscript with significant input from Dr. Tortell. A version of Chapter 3 is currently in preparation for submission to a scientific journal.

Table of Contents

ABSTRACT	ii
PREFACE	iv
TABLE OF CONTENTS	v
LIST OF TABLES	ix
LIST OF FIGURES	x
LIST OF SYMBOLS AND ABBREVIATIONS	xi
ACKNOWLEDGEMENTS	xiv
DEDICATION	xvi
CHAPTER 1: INTRODUCTION	1
1.1 BIOLOGICAL ROLES FOR DMS/P	2
1.2 CLIMATE EFFECTS OF DMS EMISSIONS.....	3
1.3 DMS/P IN POLAR REGIONS	4
1.4 THESIS OVERVIEW	5
CHAPTER 2: TOWARDS A REVISED CLIMATOLOGY OF SUMMER-TIME DIMETHYLSULFIDE CONCENTRATIONS AND SEA-AIR FLUXES IN THE SOUTHERN OCEAN.....	6
2.1 INTRODUCTION	6
2.2 METHODS	9
2.2.1 DATA DESCRIPTION	9

2.2.2	CONSTRUCTION OF THE SUMMER CLIMATOLOGY	11
2.2.3	DATA FILTERING AND SELECTION	13
2.2.3.1	DATA BINNING.....	14
2.2.3.2	CREATION OF FIRST GUESS FIELDS	15
2.2.3.3	BARNES INTERPOLATION	16
2.2.3.4	COMPARISON OF DIFFERENT CLIMATOLOGIES.....	18
2.2.4	CLIMATOOGICAL SEA-AIR DMS FLUXES	18
2.2.5	CORRELATIONS WITH ANCILLARY OCEANOGRAPHIC VARIABLES	20
2.3	RESULTS	21
2.3.1	DATA DISTRIBUTION AND CONCENTRATION TRENDS	21
2.3.2	UPDATED DMS CLIMATOLOGY	22
2.3.2.1	SURFACE-WATER DMS CONCENTRATIONS	22
2.3.2.2	SEA-AIR FLUXES	23
2.3.2.3	COMPARISON WITH L11	24
2.3.3	CORRELATIONS WITH ANCILLARY VARIABLES	25
2.4	DISCUSSION	26
2.4.1	REVISED ESTIMATES OF SOUTHERN OCEAN DMS CONCENTRATIONS AND FLUXES	26
2.4.2	EFFECTS OF INTERPOLATION PARAMETERS	30
2.4.3	TOWARDS A PREDICTIVE ALGORITHM FOR SOUTHERN OCEAN DMS CONCENTRATIONS.....	31
2.4.4	TEMPORAL VARIABILITY.....	34
2.5	CONCLUSION	35

CHAPTER 3: THE DISTRIBUTION OF METHYLATED SULPHUR COMPOUNDS, DIMETHYLSULFIDE (DMS) AND DMSP, IN CANADIAN ARCTIC WATERS47

3.1	INTRODUCTION	47
3.1.1	BIOLOGICAL ROLES FOR DMS/O/P.....	47
3.1.2	DMS/O/P IN POLAR ENVIRONMENTS	48

3.1.3	ARCTIC DMS EMISSIONS IN A CHANGING ARCTIC	50
3.2	METHODS	51
3.2.1	STUDY AREA	51
3.2.2	UNDERWAY SAMPLING SYSTEMS	51
3.2.2.1	OSSCAR	52
3.2.2.2	MIMS	53
3.2.4	POST-PROCESSING OF DMS DATA	53
3.2.5	ANCILLARY SEAWATER DATA	54
3.2.6	PHYTOPLANKTON BIOMASS AND TAXONOMIC COMPOSITION	54
3.2.7	DMS SEA-AIR FLUX.....	55
3.3	RESULTS	56
3.3.1	OCEANOGRAPHIC SETTING	56
3.3.2	OBSERVED DMS/P CONCENTRATION RANGES.....	56
3.3.3	COMPARISON OF GRADIENTS IN DMS DATA WITH HYDROGRAPHIC FEATURES	57
3.3.4	CORRELATION WITH ANCILLARY OCEANOGRAPHIC VARIABLES	59
3.3.5	PHYTOPLANKTON TAXONOMIC DISTRIBUTION.....	60
3.3.6	COMPARISON WITH THE PMEL DATABASE	61
3.3.7	DMS SEA-AIR FLUX.....	62
3.4	DISCUSSION	62
3.4.1	COMPARISON WITH EXISTING MEASUREMENTS	63
3.4.2	COMPARABILITY OF MIMS AND OSSCAR MEASUREMENTS.....	64
3.4.3	GRADIENTS IN DMS AND HYDROGRAPHIC FRONTAL STRUCTURES	65
3.4.4	PHYTOPLANKTON ASSEMBLAGE COMPOSITION AND MIXED LAYER DEPTH	66
3.4.5	THE INTERACTION OF DMS/P AND SEA ICE	67
3.4.6	DMS IN A CHANGING ARCTIC	68
3.5	CONCLUSION	69

CHAPTER 4: CONCLUSION.....	80
4.1 MAJOR FINDINGS AND CONTRIBUTIONS.....	80
4.2 FUTURE DIRECTIONS	81
BIBLIOGRAPHY.....	83

List of Tables

Table 2.1	Data Coverage by Longhurst Province for Both Datasets.....	37
Table 2.2	Pearson Correlation Coefficients of DMS and Hydrographic Variables	37
Table 3.1	Pearson Correlation Coefficients of DMS/P and Hydrographic Variables	70
Table 3.2	HPLC marker Pigments and Associated Phytoplankton Taxa	70
Table 3.3	Station Data (MLD, Ice Cover, HPLC Pigments)	71
Table 3.4	CHEMTAX-derived phytoplankton assemblage estimates.....	72
Table 3.5	An Overview of Past Summer Canadian Arctic DMS Studies	73

List of Figures

Figure 2.1 Spatial Distribution of Summertime Southern Ocean DMS Measurements	38
Figure 2.2 Latitudinal Distribution of DMS Observations	39
Figure 2.3 Monthly Distribution of DMS Measurements in PMEL and MIMS Datasets	40
Figure 2.4 Climatological Mixed-Layer Depth and Satellite Chl <i>a</i>	41
Figure 2.5 Relative Frequency Distribution of DMS Concentrations	42
Figure 2.6 Comparison of Surface DMS Climatologies.....	43
Figure 2.7 Effects of Varying Interpolation Radius.....	44
Figure 2.8 Climatological Wind Speeds and DMS Sea-Air Fluxes.....	45
Figure 2.9 Mean Difference in DMS Concentrations and Sea-Air Fluxes	46
Figure 3.1 Spatial Distribution of DMS/P and Hydrographic Variables	74
Figure 3.2 Cruise Track Record of DMS and Hydrographic Variables	75
Figure 3.3 Cruise Track Record of MIMS and OSSCAR DMS/P Measurements	76
Figure 3.4 Gradients in DMS and Hydrographic Variables.....	77
Figure 3.5 Comparison of OSSCAR-Measured DMS with PMEL Database	78
Figure 3.6 Cruise Track Record of Seawater DMS, Wind Speed, and DMS Flux.....	79

List of Symbols and Abbreviations

ACC: Antarctic Circumpolar Current

ANTA: Antarctic

APLR: Austral Polar Province

AS: Amundsen Sea

BB: Baffin Bay

CCN: cloud condensation nuclei

chl *a*: chlorophyll *a* pigment

CLAW: Charleson et al's 1987 DMS feedback hypothesis

DMS: dimethyl sulfide

DMS/O/P: dimethyl sulfide, dimethylsulfoniopropionate, and dimethyl sulfoxide

DMSO: dimethyl sulfoxide

DMSOd: dissolved dimethyl sulfoxide

DMSOt: total dimethyl sulfoxide

DMS/P: dimethyl sulfide and dimethylsulfoniopropionate

DMSP: dimethylsulfoniopropionate

DMSP: chl *a*: dimethylsulfoniopropionate to chlorophyll *a* pigment ratio

DMSPd: dissolved dimethylsulfoniopropionate

DMSPt: total dimethylsulfoniopropionate

DMSPp: particulate dimethylsulfoniopropionate

FLR: Chl-*a* fluorescence

GC: gas chromatography

HCl: Hydrogen Chloride

HNLC: High Nutrient Low Chlorophyll

Hz: hertz

I_0 : sea surface irradiance level

km: kilometer

k_d : extinction coefficient

L11: Lana 2011 DMS climatology

M: molar

m/z: mass-to-charge ratio

mE: microEinstein

MLD: mixed layer depth

MIMS: Membrane Inlet Mass Spectrometry

μg : microgram

mm: millimeter

ml: milliliter

MLD: mixed layer depth

N_2 : nitrogen

NaOH: sodium hydroxide

nM: nanomolar

NO_3^- , surface nitrate concentrations

NOAA: National Oceanic and Atmospheric Administration

NCAR: National Center for Atmospheric Research

NCEP: National Center for Environmental Prediction

OSSCAR: Organic Sulphur Sequential Chemical Analysis Robot

PAR: photosynthetically available radiation

pCO₂: carbon dioxide partial pressure

PMEL: Pacific Marine Environmental Laboratory

psu: practical salinity units

Qc.: Québec

RS: Ross Sea

S: sulphur

SANT: Subantarctic Water Ring

SRD: solar radiation dose

SST: sea surface temperature

SSTC: South Subtropical Convergence

SW: seawater concentration

Tg: teragram

WAP: West Antarctic Peninsula

WOA: World Ocean Atlas

ΔT : change in temperature

$\Delta\sigma\theta$: change in density from surface

Acknowledgements

I would like to thank my supervisor, Dr. Philippe Tortell, for a thorough and inspiring introduction into oceanography, and for his guidance and intellectual and logistical support throughout this project. I would also like to thank Dr. John Dacey for sharing his broad knowledge of electronics and chromatography (and poetry, and history, and many other things besides). Thank you as well to Dr. Susan Allen, Dr. Nadja Steiner, and Dr. Phil Austin for broadening my horizons immensely (or, rather, for making me aware that there were in fact horizons) in the fascinating field of numerical modeling of ocean and climate problems. Thank you very much to Dr. Kristin Orians and Dr. Sean Crowe for their revision of this thesis, and to my past supervisors, Dr. Elena Bennett and Dr. David Vačkář, for their continued support.

Of course, the data presented here owes a huge debt to the captains and crews of the *CCGS J.P. Tully* and *CCGS Amundsen*, as well as to the scientists at IOS. Thank you (et merci!) for making this work possible. Thank you as well to the Levasseur lab group, especially Martine and Rachel, for your gracious help. Thank you very much to Maureen Soon, and to all labmates. Lizzy – thanks for your patience in teaching me about OSSCAR’s advantages and particularities, slab climbing, and Texas country. Nina- thanks for your advice, phytoplankton help of all sorts, tolerance, and Walter. Amundsen’s Daves – thanks for insightful conversations, morale-boosting, and memorable dance moves. Anna, Ania, Alysia, Dave, Eva, Iselle, Kang, Jinghuan, Lindsey, Manuel, and Robert - thank you for your help, shared experiences, and stories.

Thank you to Tove Jansson and Philip Pullman for my early fascination with the North. Thank you to Tomáš Dvořák of Amanita Design for providing the soundscape to much of the data analysis and instrument-tinkering contained in this thesis. Thank you to my exceptional

partner Alex, for his tremendous, Alex-like support during this project. Finally, throughout this undertaking, I've come to realize I owe a great debt of gratitude to my family and close friends, who have made my corner of the world a wonderful one. To the people that I am grateful to know, who are often 3793, 3881, 8254, or even 8411 kilometers far away but also, in some often-cited way, very close- thank you, for your friendship, and words, and perspectives.

To Alena, Michal, Zdeňka, Jiří, and Jakub

Chapter 1: Introduction

Dimethylsulfide (DMS) and dimethylsulfoniopropionate (DMSP) are biogenic sulphur compounds synthesised by several species of phytoplankton and bacteria in the global ocean. DMSP acts as a cellular osmolyte in several species of marine algae and is implicated in several other cellular metabolic functions, including cryoprotection and antioxidance, under various environmental conditions. DMS is a volatile gas produced from DMSP by multiple algal and bacterial pathways in marine algal cells and in the surface ocean water column.

With a mean global concentration of ~ 4 nM, DMS is supersaturated in the water column, resulting in its rapid ventilation to the atmosphere [1]. There, it is oxidized to form climate-active sulphur compounds that alter the amount of solar radiation reaching the Earth by scattering solar energy and by serving as condensation nuclei for clouds that influence the Earth's surface albedo [2]. DMS is the largest natural source of sulphur to the atmosphere, accounting for up to 80% of the global biogenic sulphur flux [3]. A seminal hypothesis by Charlson et al, named CLAW after its authors' initials, suggests that the compounds formed from DMS in the atmosphere may have a cooling effect by playing a key role in cloud formation, creating cloud condensation nuclei (CCN) that scatter incoming radiation and alter climate patterns to affect species composition, thus creating a regional climate feedback loop [4].

Since its publication in 1987, the CLAW hypothesis has provided motivation for the study of the global concentrations of DMS and its precursors. Today, the PMEL (Pacific Marine Environmental Laboratory) database of global DMS and DMSP measurements contains over 48,000 DMS observations, and a global climatology of monthly DMS concentration was constructed by Lana et al based on these observations [1]. However, significant gaps still exist in

the understanding of the drivers of DMS/P concentrations in the water column, in the distribution of these compounds, and in the characterization of DMS flux to the atmosphere.

This thesis aims to contribute to the understanding of the distribution of DMS through studies in two polar regions: the Southern Ocean, and the Canadian sector of the Arctic Ocean. Below, I introduce biological and climate roles for reduced sulphur, and briefly discuss factors driving the distribution of DMS and DMSP in the two polar regions. Following this context, I describe the contributions of the two polar studies that make up the thesis.

1.1 Biological roles for DMS/P

DMS and DMSP are part of a biogeochemical cycle that includes multiple sulphur compounds that interact through numerous biotic and abiotic processes. The main precursor of DMS is the algal metabolite DMSP ($((\text{CH}_3)_2\text{S}^+\text{CH}_2\text{CH}_2\text{COO}^-)$), which represents the majority of the marine reduced sulfur pool [5]. In both phytoplankton and plants, DMSP is intracellularly synthesized from the amino acid methionine, but levels of intracellular DMSP can vary by up to 3 orders of magnitude between phytoplankton species [6], meaning that DMSP production cannot be simply measured by the commonly used primary-productivity proxy - chlorophyll *a* (chl *a*). In effect, this means that DMS cannot be estimated using remote sensing techniques, and must be measured in situ. Recent work has focused on identifying intracellular roles for DMSP, which has been suggested to function as an osmolyte, an anti-oxidant, and a cryoprotectant under different environmental conditions, and on determining drivers of elevated DMSP production. Sunda et al suggested that oxidative stressors, such as high solar radiation or iron limitation, may stimulate DMSP production in certain phytoplankton species [7]. After synthesis, DMSP can be cleaved to DMS and acrylate within phytoplankton cells, or by heterotrophic bacteria in the

water column [8]. Following cleavage from DMSP, DMS can be lost from the water column through three pathways: photochemical oxidation, biological DMS consumption, and ventilation to the atmosphere. The first two of these three pathways can yield the compound dimethylsulfoxide (DMSO), which, though presently understudied, has been shown to be ubiquitous in surface waters, and which may play cryoprotective and photoprotective roles in several species of phytoplankton [9].

Comprehensive reviews of the marine reduced sulphur cycle have been written recently by Stefels (2007) [10], and Yoch (2002) [11]. Though the above summary is not a complete synopsis, it highlights the large amount of factors present in the reduced sulphur web, and the consequential difficulty in predicting DMS and DMSP concentrations from easily measurable hydrographic variables. This has motivated extensive global sampling efforts, which are summarized in the climatology constructed by Lana et al.

1.2 Climate effects of DMS emissions

One objective of the global measurement of reduced sulphur concentrations is the estimation of the magnitude of sulphur emissions to the atmosphere. Both the estimation of the magnitude DMS emissions to the atmosphere and the subsequent effect of these emissions on CCN formation are active areas of research. Recently, the CLAW hypothesis has been reevaluated by several researchers, notably Quinn and Bates, who suggest that the effect of DMS emissions on CCN may not be as strong as initially thought, based on observations and modelling studies that have shown only a low DMS-induced stimulus of CCN formation [12]. However, other researchers have shown a link between DMS emissions and new aerosols in the high latitude regions, [13,14], and Quinn's paper posits that the magnitude of the effect of ocean-

derived aerosol production on CCN may be elevated during periods of high windspeed in regions with low native aerosol concentrations, such as the Arctic and Antarctic. Though the fate of DMS in the atmosphere is not the focus of this thesis, the recent debate on this topic underscores the importance of continued research in this field.

1.3 DMS/P in Polar Regions

Modelling studies and observations that show the potentially heightened importance of DMS emissions in polar regions motivate the further quantification of the marine sulphur cycle in Arctic regions. However, partly due to logistical constraints associated with sampling, these areas remain relatively sparsely sampled for DMS/P/O concentrations, and of the approximately 48,000 data points in the global Pacific Marine Environmental Laboratory (PMEL) database of oceanic DMS measurements (<http://saga.pmel.noaa.gov/dms/>) only 5% have been made in either Arctic or Antarctic waters (~ 2600 and 1000 data points, respectively). Southern Ocean DMS concentrations are roughly ~3 times higher than Arctic Ocean ones (~9 nM compared to ~3nM), with several instances of extraordinarily high DMS concentrations (>100 nM) reported, while no study to date has observed DMS concentrations above 20 nM in Arctic waters. The available data thus suggest contrasting dynamics of DMS/P production in the two polar regions.

Though the two polar oceans share several key physical characteristics, most notably strong seasonal cycles in sea ice cover and solar irradiance, there are some critical differences. Much of the Southern Ocean is an iron-limited, high nutrient low chlorophyll (HNLC) regime, with strong seasonal changes in mixed layer depths, both factors that may induce oxidative stress and thus promote high DMS production [7]. Furthermore, regions of the Southern Ocean are characterized by extremely high biomass of *Phaeocystis antarctica*, a colonial haptophyte with

extraordinarily high intracellular DMSP levels. By comparison, the highly stratified surface waters of the Arctic Ocean are believed to be primarily limited by macronutrients (i.e. nitrate), with a maximum phytoplankton biomass that is at least an order of magnitude lower than that observed in the Southern Ocean. Despite the relatively low phytoplankton biomass in Arctic marine waters, reasonably high summertime DMS levels (max ~ 20nM) have been observed in these systems, possibly as a result of light-induced oxidative stress in salinity stratified mixed layers.

1.4 Thesis overview

This thesis is comprised of two research papers, each of which makes up an individual chapter. The first paper (Chapter 2), presents a revised summertime climatology of DMS concentrations and sea-air fluxes in the Southern Ocean, based on the inclusion of new data taken using a high-frequency sampling instrument, the Membrane Inlet Mass Spectrometer (MIMS). The second paper (Chapter 3) presents new DMS and DMSP measurements made in the Canadian sector of the Arctic Ocean on the 2015 GEOTRACES expedition, as well as estimates of DMS sea-air fluxes and hydrographic data that presents some potential explanations for these observed distributions. Together, the two chapters add to the current state of knowledge of reduced sulphur concentrations in polar regions, and provide a baseline for future research in this area.

Chapter 2: Towards a revised climatology of summer-time dimethylsulfide concentrations and sea-air fluxes in the Southern Ocean

2.1 Introduction

Dimethylsulfide (DMS) is a biogenic gas produced by various marine ecosystem processes [15] and rapidly ventilated to the atmosphere, where it is oxidised to form climate-active sulfur compounds.[16,17] The precursor of DMS is the algal compound dimethylsulfoniopropionate (DMSP), which serves important physiological functions, including suggested roles as a cellular cryoprotectant, osmolyte and antioxidant under various environmental conditions.[18] A seminal hypothesis put forth by Charlson et al.[4] suggests that DMS-derived oxidation products play a role in controlling regional climate by altering atmospheric acidity and promoting cloud condensation nuclei that scatter incoming radiation. Although the strength of this potential climate feedback is currently under debate,[12] it is clear that oceanic DMS emissions significantly influence atmospheric radiative balances on regional scales,[16,17] and this has prompted significant research into the factors driving DMS accumulation across the global oceans.

DMS concentrations have been measured in surface ocean waters for over four decades. In recent years, several groups have made efforts to synthesise these observations into global climatologies that capture the mean spatial and temporal patterns of oceanic DMS concentrations, and the underlying relationships between DMS and other biogeochemical variables. The first global DMS climatology, produced by Kettle et al., [3] served as a benchmark for the DMS research community and was used to validate models predicting

surface-ocean DMS concentrations and climate-dependent responses of oceanic DMS fluxes. [19-21] Since the publication of this original climatology, the global database of surface-ocean DMS measurements has expanded significantly, and an updated climatology was recently produced by Lana et al. in 2011[1] (hereafter referred to as L11). Although the original and updated climatologies exhibited some differences in the magnitude of surface-ocean DMS concentrations and sea-air fluxes, the overall regional patterns observed by Kettle et al.[3] were preserved in the updated L11 climatology. Most notably, both the original and updated climatologies identified several oceanic regions of high summertime DMS concentrations, particularly in the Southern Ocean.

There are several potential explanations for the persistence of summertime DMS hot-spots in the Southern Ocean. These include the abundance of high-DMSP-producing *Phaeocystis antarctica* [22] and the presence of iron-limiting conditions,[23,24] which may stimulate DMSP and DMS production by inducing cellular oxidative stress.[7] Additional oxidative stress may result from the presence of high UV fluxes around the Antarctic continent.[25] Although a definitive explanation for the elevated DMS and DMSP concentrations in the Southern Ocean is lacking, the significance of this region to global ocean DMS emissions is now clear.

Relative to many oceanic regions, the vast expanse of the Southern Ocean remains largely undersampled. The scarcity of data results, in large part, from the remoteness of much of the Southern Ocean, and the significant logistical constraints on the operation of research vessels in polar waters. Although significant DMS data coverage does exist for several Southern Ocean locations, particularly in the Ross Sea and in close proximity to major research stations, large observational gaps remain. The undersampled areas represent several distinct biogeochemical regimes, where different factors control productivity and biogenic gas production. For example,

iron limitation is known to control summertime productivity and phytoplankton species assemblage composition in much of the off-shore pelagic realm,[24] whereas biogeochemical dynamics in iron-rich continental shelf waters are strongly influenced by sea-ice processes.[26] Such strong regional differences in the factors driving DMS cycling make it challenging to extrapolate DMS observations across sparsely sampled Southern Ocean waters. Based on the recent increase in Southern Ocean DMS data, L11 concluded that the original climatology of Kettle et al.[3] significantly overestimated DMS concentrations and sea–air fluxes in this region. The difference between the original and updated Southern Ocean DMS climatologies has important implications for regional S budgets, and underscores the importance of increased data coverage in this critical region.

Over the past decade, new technological developments have begun to address the need for increased DMS observations across the Southern Ocean and other key oceanographic regions. In particular, the development of membrane inlet mass spectrometry(MIMS[27]), and related analytical systems[28] has enabled very high-frequency DMS observations, and facilitated high-resolution mapping of surface water DMS concentrations. These emerging data sets have provided new insights into fine-scale DMS variability in contrasting Southern Ocean regions, and the underlying relationships with various biogeochemical factors (e.g. Tortell et al.[29,30]). Thus far, however, the rapidly growing data set of MIMS-based Southern Ocean DMS measurements has not been systematically examined to assess larger-scale regional patterns. The new data thus present an opportunity to re-evaluate the existing Southern Ocean DMS climatology. In the present article, we present an updated DMS climatology for the Southern Ocean, examining how the inclusion of recently available MIMS data affects the mean derived climatological concentrations and sea–air fluxes. To facilitate comparison with existing

climatologies, we employed a method of objective analysis based on that of L11, with specific modifications aimed at adapting the approach to a regional Southern Ocean study. Our results demonstrate how the inclusion of new data and the use of region-specific methodology influence the derived DMS climatology across various Southern Ocean areas. We explore the relationships between the updated DMS data and a variety of ancillary hydrographic and biogeochemical variables.

2.2 Methods

2.2.1 Data Description

As a starting point for the climatology, we used the Pacific Marine Environmental Laboratory (PMEL) database of ~48,000 global DMS measurements (<http://saga.pmel.noaa.gov/dms/>, accessed September 2015). Of these observations, 7,500 data points fall within the Southern Ocean, defined here as waters south of 40°S. As our focus is on summertime observations (corresponding to the period of maximum DMS concentrations and sea–air fluxes; L11[1]), we only utilise Southern Ocean measurements obtained between December and February (justification for the inclusion of only these 3 months is given below).

This resulted in a final data set of ~2600 summertime PMEL observations obtained between 1987 and 2009. By comparison, repeated MIMS surveys in the Southern Ocean between 2006 and 2013 have yielded more than 700 000 summertime (Dec–Feb) DMS measurements. As discussed below, not all of these measurements should be considered statistically independent, given the high spatial resolution of the data collection. The MIMS data come from published studies,[29-31] with the exception of two cruises – one transect from Cape Town to Punta Arenas (via the Weddell Sea and West Antarctic Peninsula) on the German vessel Polarstern in

2011, and a survey of the Ross Sea on the US ship Nathaniel B. Palmer in 2013. Detailed descriptions of these unpublished data will be presented elsewhere.

There are several caveats that need to be considered when combining MIMS and PMEL data into a single climatology. First, there are potential methodological biases between MIMS-derived underway data and those obtained using standard gas chromatographic (GC) analysis of discrete samples. Several studies comparing MIMS DMS measurements with GC-based observations have shown that the two methods produce comparable results in the Ross Sea polynya, [29] Bering Sea,[27] Subarctic Pacific[32] and West Antarctic Peninsula (L. Asher, J. Dacey and P. Tortell, unpubl. data). Within these studies, measurements derived from GC and MIMS analysis were highly correlated (Pearson's $r > 0.92$, $n = 65$), with an overall slope that was not significantly different from 1 (0.97 ± 0.05). A second potential consideration is the temporal offset between the MIMS (2006–13) and PMEL (1987–2009) data, which could lead to a potential sampling bias resulting from interannual variability. To examine this possibility, we analysed the temporal trends in summertime DMS data for both the whole Southern Ocean, and for a well-sampled region of the Ross Sea polynya. This analysis did not reveal any directional interannual variability that would bias the comparison of observations collected over a span of several decades. We thus conclude that MIMS and GC data can, indeed, be reasonably combined into a single database in order to construct a revised Southern Ocean DMS climatology.

The spatial distribution of all DMS concentration measurements used in our analysis (both PMEL and MIMS) is shown in Fig. 2.1. Some regions, including the Ross Sea (RS) and West Antarctic Peninsula (WAP), are reasonably well sampled in both data sets. However, the MIMS data fill in important gaps in regions such as the Amundsen Sea (AS), and provide new observations along several meridional transects (e.g. south of Tasmania and South Africa). As

shown in Fig. 2.2, there is a significant difference in the latitudinal distribution of Southern Ocean DMS measurements in the PMEL and MIMS data. The large majority of MIMS data were obtained in waters south of 55°S (mostly south of the Polar Front; see Fig. 2.1), whereas a significant fraction of the PMEL data represents waters between 55 and 40°S (between the Subtropical and Polar Fronts).

2.2.2 Construction of the summer climatology

We created an interpolated map of summertime DMS concentrations, using the general approach of L11. In the following sections, we provide specific information on each step in our analysis, with particular attention to areas where our methods differ from those of L11. The general approach is based on creating a gridded mean DMS field based on actual observations, and using this to derive first-guess values assigned to different biogeographic regions of the Southern Ocean. These first-guess values are then combined with actual observations to create a smoothed and interpolated climatological map.

As noted above, we diverged from the approach of L11 in our treatment of monthly DMS data. Whereas L11 created a series of monthly interpolated DMS climatologies, we have opted to create a single climatology for the austral summer. We chose this approach both because MIMS data are only available in the summer months, and owing to the sparse monthly data coverage for the Southern Ocean, which is illustrated in Fig. 2.3. The extent to which DMS data from different months can be reasonably combined into a single mean summer value depends on the similarity of DMS concentrations and other environmental conditions across these months. To assess oceanographic conditions across the summer months, we examined the monthly climatology of Southern Ocean chlorophyll-a (chl *a*) distributions and mixed-layer depths

(www.ifremer.fr/cerweb/deboyer/mld, accessed September 2015) between November and February. The chl *a* climatology was derived from AquaModis Level 3 observations (<http://oceancolor.gsfc.nasa.gov/cgi/l3>, accessed September 2015) using the Southern Ocean-specific processing algorithm of Johnson et al.[33] The mixed-layer depth climatology [34] is derived from an analysis of all available hydrographic data over the past several decades, based on threshold temperature difference (ΔT) of 0.2°C or density difference ($\Delta\sigma\theta$) of 0.03 kg m⁻³ from near-surface (10 m) values.

As shown in Fig. 4, Southern Ocean mixed-layer depths, sea-ice cover (as inferred from missing oceanic data in monthly chl *a* climatological maps) and phytoplankton biomass are broadly similar for December, January and February. North of the Polar Front, mixed layers are somewhat deeper in December than in January and February, but values are more similar across all 3 months closer to the Antarctic continent. In contrast, chl *a* concentrations, sea-ice cover and mixed-layer depths in November (Fig. 2.4a, b) are distinctly different from those observed between December and February. Chl *a* is significantly lower in November, owing in large part to increased sea-ice cover and significantly greater mixed-layer depths. These results highlight the broad similarity in hydrography and phytoplankton biomass distributions during the peak summer months (Dec–Feb), and provide justification for constructing a mean summertime DMS climatology based on observations collected during these 3 months.

Comparison of monthly Southern Ocean DMS frequency distributions (Fig. 2.5) provides further support for the construction of a mean summertime DMS climatology, based on an average of Dec–Feb data. The distribution of DMS concentrations shows broad similarity between December and February, with distributions centred around 3 nM and a long tail towards high concentrations. There is, however, a larger proportion of very high (100 nM) DMS

observations in January, and a greater frequency of low (1 nM) DMS measurements in February. The high January DMS data are largely derived from the PMEL database, and these values were removed in the original L11 analysis by a data cut-off filter (see below). Given the limited data coverage for February (Fig. 2.3), the greater frequency of low DMS values may simply reflect a sampling artefact (e.g. very few Ross Sea observations), rather than a true difference in the underlying data distribution. In light of the similarity of other oceanographic variables between December and February, (Fig. 2.4), we thus believe that a combined summertime DMS climatology is the best approach until additional data become available for individual months. We also note that L11 used Dec–Feb average values when comparing their updated climatology with that of Kettle et al. [3]

The exclusion of November data from the summer climatology, which we justify based on differences in surface–ocean properties (Fig. 4), does not have a significant effect on our results. Within the limited scope of the November data, we found mean DMS concentrations and sea–air fluxes for $1 \times 1^\circ$ averaged bins (described below) were similar to those derived from the Dec–Feb averages. Moreover, the small number of November observations (Fig. 2.3) limits the statistical significance of these data on the overall summertime average.

2.2.3 Data filtering and selection

As pointed out by previous authors (e.g. Kiene and Slezak [35]), DMS concentration measurements are subject to potential sampling artefacts derived from cell lysis and the release of DMSP lyase, which catalyses the transformation of DMSP into DMS.[36] It is thus possible that continuous seawater pumping systems, as used for underway MIMS analysis, may contribute to these artefacts, yielding anomalously high DMS values. As discussed above, direct

comparisons between MIMS DMS measurements and those derived from discrete bottle samples have shown good general agreement between these methods, suggesting that cell lysis artefacts do not specifically bias MIMS data.

In the analysis of L11, data were filtered to remove all values above the 99.9% percentile of global measurements, resulting in a cut-off value of 142 nM. The use of a globally defined cut-off is potentially problematic in the Southern Ocean where very high DMS concentrations are commonly reported. Examination of the Southern Ocean DMS frequency distribution (Fig. 2.5b) shows that ~0.5% of all DMS observations (all summer data for both MIMS and PMEL) exceed the 142 nM global cut-off. Although it is impossible to say how many of these values may represent sampling artefacts, anecdotal evidence (based on the smell of marine air) suggests that extremely high DMS concentrations are a real feature of some Southern Ocean waters, including *Phaeocystis* blooms in the Ross Sea.[37] For our analysis, we thus derived a 99.9% cut-off value specific for the Southern Ocean, removing all data with DMS concentrations in excess of 320 nM. In our analysis, we examine the effect of the different data cut-offs on the resulting climatologies.

2.2.3.1 Data Binning

To standardise the interpolation field and facilitate further analysis, observations from the combined PMEL and MIMS databases were averaged into 1° x 1° bins, following the approach of L11. This averaging procedure is potentially subject to a strong sampling bias, due to the very high number of MIMS data points. In grid cells containing both MIMS and PMEL observations, the potentially large number of MIMS observations (many of which represent repeated measurements within a single local water mass) could overwhelm the sparser PMEL data points,

biasing the resulting average value towards the MIMS measurements. To address this, we derived separate $1^\circ \times 1^\circ$ binned averages for the MIMS and PMEL data, and used these values to derive an overall grid cell mean. The final grid cell mean was obtained from a weighted average of the PMEL and MIMS data, where the weighting was determined by the number of individual years with MIMS or PMEL data. For example, in a grid cell with 7 years of PMEL data and 4 years of MIMS data, the grid cell average PMEL and MIMS values would receive weighting factors of 7/11 and 4/11 respectively. This approach effectively treats mean grid cell DMS measurements from different years as independent data points, and corrects for the high sampling frequency of the MIMS data.

2.2.3.2 Creation of first guess fields

The method of interpolation selected by L11 requires an initial ‘first-guess’ value at every point in the field to be interpolated. We followed the approach of L11 in deriving this first-guess field by categorising primary data into ecological provinces as defined by Longhurst. [38] The geographical limits of the Longhurst provinces were obtained from a publicly available marine georeferencing database (<http://www.marine-regions.org/sources.php>, accessed October 2014). There are four provinces that fall within the domain of the Southern Ocean (SSTC, SANT, ANTA, APLR; provinces 51–54; see Table 2.1 legend for full names of provinces), and we computed the average summer DMS concentration for each of these provinces based on our $1^\circ \times 1^\circ$ gridded data set. Because the MIMS data do not contain any new observations in the south Indian Ocean, we also computed basin-specific first-guess values for each ecological province in the Atlantic, Pacific and Indian Ocean basins, to avoid changing the first-guess field in regions with no new measurements. The latitudinal and longitudinal boundaries of these three

ocean basins were based on the definitions provided by the International Hydrographic Bureau.[39] The first-guess values for the Atlantic and Pacific Oceans were derived from the combined MIMS and PMEL data sets, whereas the Indian Ocean first-guess field was derived exclusively from PMEL observations.

Following the approach of L11, we used an unweighted Shuman filter to smooth the boundary edges of the first-guess fields, to eliminate sharp discontinuities that would cause abnormalities in the interpolation. In the unweighted form of the Shuman filter, each data point is the simple average of a neighbourhood of points that symmetrically surround it, with the point size of the filter determining the size of the neighbourhood. Whereas L11 used an 11-point filter (i.e. neighbourhood of 11 by 11 points, centred on the observation of interest), we used a seven-point filter based on a subjective evaluation of the resulting first-guess fields. In practice, we found that the size of this smoothing filter applied to the first-guess field had only a small effect on the resulting climatology, because it only affects grid cells in close proximity to the boundary edges.

2.2.3.3 Barnes Interpolation

In creating their final DMS climatology, L11 utilise the distance-weighted interpolation scheme of Barnes et al.,[40] applying the algorithm according to Locarnini et al.[41] In a Barnes interpolation, the first-guess field at any point (the province average value) is corrected based on the values of actual data points within a chosen radius of influence. A distance weighting scheme is used, such that the influence of data used in the correction term decreases with increasing distance. The explicit form for the correction factor C at each point is:

$$C = \frac{\sum_{s=1}^n W_s Q_s}{\sum_{s=1}^n W_s} \quad (1)$$

where s is an observation within the radius of influence from the bin in question, n is the total number of observations within the radius, W is the Gaussian distance weighting function,[40] and Q is the difference between the observation and the first-guess field. Thus, the correction factor at each bin is the sum of the distance-weighted corrections within the area of influence, and the final climatological value is derived from the sum of the first-guess values and the correction factor. Following L11, we applied the Barnes interpolation for all grid cells, including those that contained primary measurements. As a result, all grid cells in our final climatology represent interpolated values.

From the form of the correction factor (Eqn. 1), it can be seen that the radius of influence determines the number of points that are considered by the algorithm, and thus the extent to which data are smoothed across space. In their analysis of global DMS distributions, L11 chose a 555-km radius of interpolation. As a starting point, we also used a 555-km radius in our Barnes interpolation. However, we found that this value produced significant ‘smearing’ of DMS across distinct Southern Ocean hydrographic regions. We thus experimented with a range of interpolation radii, seeking to reproduce regional features, while also obtaining reasonable smoothing across the sparse data grid. In our final analysis, we chose a radius of 140 km, which is approximately 4-fold lower than that used by L11. This smaller value is consistent with the 4-fold-lower Rossby radius of deformation in high-latitude regions, as compared with the global average. The Rossby radius is a characteristic length scale for spatial heterogeneity, and thus provides a reasonable metric for spatial smoothing in the climatology.

Following the Barnes interpolation, the resulting data were further smoothed to minimize spatial discontinuities. L11 used a two-step smoothing procedure, first applying a median filter, and then an 11-point Shuman filter. In our analysis, we chose to omit the median filter step, because this intrinsically removes the highest values, which may represent localized DMS features. We thus only used a single-pass 5-point Shuman filter to smooth the climatology. As a result of the somewhat different smoothing method we used, our climatology shows more heterogeneous DMS distributions than that of L11 (see Results section).

2.2.3.4 Comparison of different climatologies

For comparative purposes, we applied our objective analysis methods to produce two primary climatologies – one based on the original PMEL data set (used by L11), and the other based on our updated data set (MIMS . PMEL). Both of these climatologies were produced using a Barnes interpolation radius of 140 km and a data cut-off of 320 nM. In order to examine additional methodological biases, we also produced a climatology from the updated data set with the larger (555-km) interpolation radius used by L11. For more direct comparison of our updated climatology with the work of L11, we obtained a gridded data field of the original L11 monthly climatology (http://www.bodc.ac.uk/solas_integration/implementation_products/group1/dms/, accessed August 2014) and used this to generate a Dec–Feb average DMS concentration field.

2.2.4 Climatological sea-air DMS fluxes.

We derived sea–air fluxes of DMS using our climatological maps of surface-water DMS concentrations, in conjunction with climatological wind speed and sea-ice data. Relative to L11,

we used a simplified approach to compute sea–air DMS fluxes based on water-side resistance only. L11 showed that this simplified approach produces results that agree to within better than 10% with calculations that include both water-side and air-side resistance. This error is relatively small compared with the uncertainty associated with the calculation of sea–air exchange coefficients, particularly in ice-covered regions. We thus feel that a simplified approach is justified, and we focus on the comparison of different flux climatologies rather than the absolute values. We computed sea–air flux (FDMS) as:

$$FDMS = kDMS(DMS_{sw}) (1 - A)^{0.4}$$

where DMS_{sw} is the concentration of DMS in the surface ocean and $kDMS$ is the gas transfer velocity derived from the equations of Nightingale et al., [42] normalised to the temperature and salinity-dependent DMS Schmidt number of Saltzman et al.,[43] and A is percentage sea-ice cover. The scaling exponent of 0.4 accounts for the effects of sea ice on gas exchange and is derived from the work of Loose et al.[44] Monthly sea surface temperature (National Oceanic and Atmospheric Administration’s NOAA Optimum Interpolation SST V2), wind speed and sea ice (percentage cover) data used in the flux calculations were derived from the National Center for Atmospheric Research (NCAR)–National Center for Environmental Prediction (NCEP) reanalysis output (<http://www.esrl.noaa.gov/psd/data/gridded/tables/ocean.html>, accessed August 2014). We computed Dec–Feb mean values between 1990 and 2014, a time interval that encapsulates 90 % of the underlying DMS data used in our study. A climatological salinity field was derived the 2009 World Ocean Atlas data (https://www.nodc.noaa.gov/OC5/WOA09/pr_woa09.html, accessed September 2011). All variables were linearly interpolated to the $1^\circ \times 1^\circ$ resolution of our climatological DMS grid. We used the same approach to derive mean summertime sea–air fluxes from the original L11

climatology, based on average summertime DMS concentrations as described above.

2.2.5 Correlations with ancillary oceanographic variables

We examined the relationship between Southern Ocean DMS concentrations and a range of oceanographic variables. For the current analysis, we utilised the underlying 1° x 1° gridded DMS data, rather than the interpolated climatology. DMS data were logarithmically transformed to account for their significant non-normal distribution. In addition to the ancillary data described above (e.g. chl *a*, mixed layer depth (MLD) and sea ice), we also extracted climatological mean values (Dec–Feb) for NO₃⁻ concentrations (World Ocean Atlas, 2009), chl *a* fluorescence yields (ϕFLR) and estimates of the relative abundance of *Phaeosystis*-like and nanoflagellate-like phytoplankton taxa. chl *a* fluorescence yields, which have been suggested as a potential metric for Southern Ocean iron limitation,[45-47] were calculated following the approach of Browning et al.[47] The relative abundance of *Phaeosystis*-like and nanoflagellate-like phytoplankton groups was derived from the output of the PHYSAT algorithm, in which broad taxonomic groups are identified based spectral pigment signatures.[48] We obtained monthly (Dec–Feb) maps of PHYSAT output between 1997 and 2010 (<http://log.cnrs.fr/Physat-2?lang=fr>), and used these to generate a mean summertime value. Finally, solar radiation dose (SRD, mE m⁻² s⁻¹) was computed following the approach of Vallina and Simo.[49]:

$$\text{SRD} = I_0 / (k_d * \text{MLD}) * (1 - e^{-(k_d * \text{MLD})}) \quad (2)$$

where I_0 and k_d represent sea surface irradiance levels and extinction coefficients, respectively.

Irradiance levels were derived from monthly climatologies of AquaModis PAR

(photosynthetically available radiation; 400 – 700 nm), while extinction coefficients were

obtained from a chlorophyll-dependent algorithm [50], which is available as an evaluation product from the AquaModis satellite (<http://oceancolor.gsfc.nasa.gov/cgi/13>).

2.3 Results

2.3.1 Data distribution and concentration trends

As shown in Table 2.1, the inclusion of MIMS data leads to a significant (>35 %) increase in the number of grid cells with primary measurements, resulting in 737 new data-containing 1° x 1° bins. As expected from the latitudinal distribution of MIMS data (Fig. 2.2), most new grid cells in the updated data set are located in the two high-latitude provinces ANTA (53) and APLR (54), where the inclusion of MIMS data increased the spatial coverage by ~60 and 40% respectively.

Fig. 5b shows the effect of MIMS data on the frequency distribution of Southern Ocean DMS concentrations. Compared with the PMEL data alone, the updated gridded data set shows a shift in the frequency distribution from ~1–10 nM towards 10–30 nM DMS, reflecting the increased representation of higher-DMS regions south of the Polar Front. In contrast, the updated data reduce the frequency peak of DMS concentrations between ~30 and 100 nM, which corresponds to Ross Sea measurements in the PMEL data (Fig. 1a). For both the original and updated data sets, a clear difference can be seen between the Southern Ocean DMS frequency distributions and the global data set, with a higher mean value and a larger proportion of Southern Ocean DMS concentrations greater than 10 nM. This difference underscores the need for a regional Southern Ocean DMS climatology.

2.3.2 Updated DMS climatology

2.3.2.1 Surface-water DMS concentrations

Fig. 6 shows the main results of our objective analysis, including the first-guess fields (Fig. 6a, c and e) and final derived climatologies (Fig. 2.6b, d and f). The top and middle row of plots in this figure compare the results of our analysis using the PMEL data (Fig. 2.6a, b) and updated data (MIMS + PMEL; Fig. 6 c, d). Both data sets shown in these panels were treated with a 320 nM cut-off value, using first-guess fields derived from the basin-specific averages of the underlying 1° x 1° gridded data. For comparative purposes, the bottom row of plots (Fig. 2.6e, f) shows the first-guess fields and resulting climatologies derived from the updated data averaged across all three Southern Ocean basins.

Comparison of Fig. 6a and 6c reveals that the inclusion of new data significantly changed the basin-specific first-guess fields in the Atlantic and Pacific sectors. In contrast, the Indian Ocean sector remained unchanged owing to the lack of new data in this region. The largest change in a first-guess field was observed in the polar region of the Pacific sector (province 54), where the inclusion of MIMS data led to a significant reduction in average Ross Sea DMS concentrations. In contrast, first-guess fields for the updated data set were higher in the polar Atlantic sector (province 54), and in the Antarctic region (province 53) of both the Atlantic and Pacific Sectors. Owing, in part, to changes in the first-guess fields, the updated climatology (Fig. 2.6d) showed lower DMS concentrations in the vicinity of the Ross Sea (Pacific sector of province 54), and higher concentrations over significant portions of province 53.

As can be seen by comparing Fig. 2.6d and 2.6f, the use of basin-specific first-guess fields for the updated data had only a modest effect on the resultant climatology in the Pacific and Atlantic sectors. In contrast, the use of province-wide averages resulted in significantly

higher first-guess fields for the Indian sector of the Southern Ocean (particularly for province 53). This higher first-guess field was then used to interpolate missing data in this region, resulting in higher climatological DMS values relative to those obtained from the basin-specific first-guess fields. Fig. 2.7 illustrates the effects of data cut-off thresholds and the Barnes interpolation radius on the resulting DMS climatology.

Comparison of Fig. 2.7a and 2.7b shows that the lower cut-off value used by L11 (142 v. 320 nM in the present study) leads to a significant reduction in derived DMS concentrations for the Ross Sea region. Outside of this area, however, there are few DMS measurements above 140 nM, and the choice of data cut-off values has little influence on the climatology. In contrast, the use of a larger Barnes interpolation radius influences the entire climatology. An interpolation radius of 555 km (as in L11) produces a smoother climatological field (Fig. 2.7c), but tends to exaggerate the extent of high-concentration features, while dampening the spatial variability observed in the underlying data (Fig. 1). In contrast, the climatology based on a 140-km interpolation radius (Fig. 2.7b) follows the underlying data structure more closely, but leaves larger areas derived from the first-guess field. Given the high heterogeneity of Southern Ocean surface waters (Figs 2.1, 2.4), we believe that a smaller interpolation radius is more appropriate for representing the regional DMS distribution.

2.3.2.2 Sea-air Fluxes

Our summertime climatology of Southern Ocean DMS concentrations can be used to derive updated regional sea-air flux estimates (Fig. 2.8). Variability in sea-air DMS flux depends not only on the underlying DMS concentration field, but also on spatial gradients in wind speed and sea-ice cover. The Southern Ocean exhibits strong meridional variability in

wind-speeds (Fig. 2.8a), with maximum values ($>10 \text{ m s}^{-1}$) between the subtropical and sub-Antarctic fronts ($\sim 40\text{--}50^\circ\text{S}$), minimum values south of the Polar Front, and increased values in some regions along the Antarctic continental shelf. Regions with high wind speeds in the sub-Antarctic region coincide with low to moderate surface-water DMS concentrations (Fig. 2.7b), resulting in reasonably elevated sea–air fluxes ($\sim 10\text{--}20 \text{ mmol m}^2 \text{ day}^{-1}$) over much of this region (Fig. 2.8b). In contrast, lower wind speeds and increased sea-ice cover closer to the Antarctic continent act to limit sea–air DMS fluxes, despite high background DMS concentrations. Nonetheless, high DMS fluxes ($>50 \text{ mmol m}^2 \text{ day}^{-1}$) are observed in several DMS hot-spots in the Ross and Weddell Seas, where climatological wind speeds range between 5 and 10 m s^{-1} . Integrating the derived fluxes over the entire Southern Ocean domain ($40\text{--}70^\circ\text{S}$), we calculate an overall summertime (Dec–Feb) sea–air flux of 3.4 Tg S. This value is compared against previous estimates in the discussion.

2.3.2.3 Comparison with L11

The high degree of spatial heterogeneity in the climatological fields (Figs 2.6–8) makes it challenging to visually compare the original and updated data products. Areas of divergence are more easily discerned in difference plots (Fig. 2.9), where our updated climatology is compared against the summertime average derived from the original climatology of L11. This comparison was chosen to contrast our results with a derived climatology that is widely used by the DMS research community. The comparison with L11 includes the effects of different data sources and treatment (cut-off threshold and smoothing functions; see Methods). In terms of DMS concentrations, the two climatologies show little differences north of 50°S , with a mean increase of only $\sim 2 \text{ nM}$ in province 51 of the updated climatology (Fig. 2.9b). However, given the very

high wind speeds of this region (Fig. 2.8a), the small increase in climatological DMS concentrations translates to notably higher sea–air fluxes (Fig. 2.9d) at latitudes north of 50°S. At higher latitudes (60–70°S), both surface-water DMS concentrations and sea–air fluxes exhibit a pronounced increase in the updated climatology (Fig. 2.9d), albeit with significant spatial variability (Fig. 2.9c). Indeed, the revised climatology shows areas of both increased and decreased DMS concentrations across provinces 53 and 54. The strongest decrease in the updated climatology relative to L11 occurs in the vicinity of the Ross Sea. In contrast, several higher concentration and sea–air flux regions are identified in the Atlantic and Pacific sectors of provinces 53 and 54. As discussed further below, some of these newly identified regional increases are spatially coherent with areas of persistently high chl *a* concentrations (Fig. 2.4), suggesting that they are significant features of the Southern Ocean.

2.3.3 Correlations with ancillary variables

We examined potential relationships between log-transformed DMS concentrations and other regional oceanographic variables by computing Pearson’s correlation coefficients (Table 2.2). For the purpose of the present analysis, we only considered grid cells that contained primary observations (as opposed to interpolated values from the climatology). We did not find strong correlations between DMS concentrations and any of the ancillary variables we examined. However, DMS concentrations did exhibit weak negative correlations with mixed-layer depth (MLD) and sea surface temperature ($r = -0.25$ and -0.22 respectively), and weak positive correlations with chl *a*, sea-ice cover, and the Chl-*a*/MLD ratio ($r = 0.25$, 0.34 and 0.24 respectively). DMS grid-cell averages also showed weak negative correlations with the inferred abundance of *Phaeocystis*-like and nanoflagellate-like phytoplankton taxa from the PHYSAT

algorithm. No correlations were observed with chl *a* fluorescence yields, NO₃⁻ concentrations, salinity or SRD. In addition to the analysis of pair-wise correlations, we followed the approach of Asher et al., [51] who used a stepwise linear regression to construct an empirical predictive model for DMS in the Subarctic Pacific, based on the ancillary oceanographic data. Using this approach, we were unable to derive a robust predictive equation, with a maximum R² value of only 0.16 (data not shown).

2.4 Discussion

Relative to the benchmark work of L11, our updated Southern Ocean DMS climatology demonstrates regions of both increased and decreased DMS concentrations and sea–air fluxes across a wide latitudinal band (~60–75°S), and reveals new hotspots of DMS accumulation in several previously unsampled regions (Fig. 2.9). Below, we discuss our results in terms of regional sulfur budgets, and consider some methodological issues associated with the construction of the climatology. We focus, in particular, on the choice of interpolation parameters and data cut-off thresholds, and on the limitations of using an average summertime climatology that does not resolve underlying temporal dynamics. We also discuss the difficulties associated with empirically predicting surface–ocean DMS concentrations from other ancillary oceanographic data.

2.4.1 Revised estimates of Southern Ocean DMS concentrations and fluxes.

One of the major conclusions of L11 was that the original climatology of Kettle et al.[3] overestimated DMS concentrations in the Southern Ocean, particularly at high latitudes (>60°S). The difference between the two climatologies was attributed to an increase in data density in the

updated PMEL archive. As shown in Fig. 2.2, however, less than 30% of Southern Ocean DMS data used by L11 were obtained at latitudes greater than 60°S, and less than 15% at latitudes pole-ward of 65°S. By comparison, nearly 90% of the MIMS measurements were obtained south of 60°S, yielding nearly 700 new data-containing grid cells in provinces 53 and 54. These new measurements thus provide valuable information for polar and sub-polar regions, where DMS concentrations are expected to be highest. The resulting updated climatology shows a mean tendency towards increased DMS concentrations relative to the L11 climatology across the two high-latitude provinces, with values increased by over 10 nM in some cases. Although the overall trend was towards an increase in the climatological DMS field between ~60 and 75°S (Fig. 2.9), the updated climatology also includes several areas (most prominently in the Ross Sea) where mean DMS concentrations decreased owing to the inclusion of new MIMS data. These regional decreases notwithstanding, we conclude that mean summertime DMS concentrations in the Southern Ocean are likely to be closer to the original estimates of Kettle et al.[3] than to the revised (lower) values obtained by L11. Clearly, significantly greater data coverage, over both space and time, is needed to more accurately represent mean DMS concentrations across the Southern Ocean. Our analysis should thus be considered as a step forward in the continued development of a more robust Southern Ocean DMS climatology.

Sea-air flux of DMS, rather than the seawater concentration, is the critical factor in determining the effects of sulfur on atmospheric radiative balance and potential climate feedbacks. In our updated climatology, we derived a total Southern Ocean DMS flux of ~3.4 Tg S over the summer season (Dec–Feb). In comparison, L11 and Kettle et al. derived mean annual fluxes of ~5.8 Tg S for the Southern Ocean latitudinal bands between 40 and 70°S. These numbers suggest that the peak summer months (Dec–Feb) account for ~60% of total annual

DMS fluxes from the Southern Ocean, and ~15% of global annual ocean DMS emissions to the atmosphere. As discussed above, we found that inclusion of November data in the climatology did not result in a significant increase in the mean summertime sea–air DMS fluxes. Despite the potential for high DMS concentrations associated with early season *Phaeocystis* blooms in (for example) the Ross Sea polynya, the presence of significant sea-ice cover (Fig. 2.4) acts to limit the ventilation of DMS to the atmosphere. Within the Southern Ocean, our analysis and that of the previous climatologies suggest that regions north of the Subarctic Front (provinces 51 and 52) contribute most strongly to sea–air DMS fluxes, owing to the very strong persistent winds in this region (Fig. 2.8a). Despite the relatively low surface-water concentrations of these Subantarctic waters, they account for ~50% of the total climatological sea–air DMS (Fig. 2.8b), making them important areas for future data collection efforts.

Despite somewhat contrasting spatial patterns of surface DMS concentrations and sea–air fluxes, the original and revised climatologies show consistent differences between these variables. Our analysis suggests that values derived from the PMEL data alone represent underestimates in high-latitude regions (Fig. 2.9). The increased climatological DMS flux in some Southern Ocean regions is consistent with the limited available observations of atmospheric DMS concentrations. Mahajan et al.[52] have shown that high atmospheric DMS mixing ratios observed in January and February at Amsterdam Island in the southern Indian Ocean cannot be reproduced by the climatological fluxes derived by Kettle et al.[3] or L11. Based on an analysis of potential source terms, these authors suggest that an increase in the oceanic DMS source term (i.e. increased sea–air flux) is needed to account for the atmospheric data. Although our revised climatology does not produce any changes in the Indian Ocean DMS fluxes (owing to a lack of new data in this area), our derived sea–air fluxes are consistent with

other direct measurements. For example, time-series observations in the Pacific sector of the Southern Ocean [53] (see box in Fig. 2.8) have yielded DMS flux estimates between ~ 3 and $4.5 \text{ mmol m}^{-2} \text{ day}^{-1}$ which are within the range of our derived climatological values (Fig. 8b).

Beyond contributing to regional atmospheric sulfur budgets, sea–air DMS fluxes are also significant at more localised scales. At these smaller scales, some areas appear to show very large (i.e. $>400 \%$) differences between the two climatologies, with both increases and decreases observed in the $1 \times 1^\circ$ binned data. The most notable decrease in the updated climatological DMS flux occurs in the Ross Sea, as noted above. This feature is significant in terms of localised deposition of S aerosols on the Antarctic continent, and the use of these deposition records to infer regional productivity and sea-ice extent.[54]

In constructing our sea–air flux climatology, we used the approach of Kettle et al.[3] and L11, combining climatological mean values for DMS concentrations, wind speeds and sea-ice cover. For the MIMS data, sea–air fluxes can be more accurately derived by computing values based on simultaneous measurements of DMS concentrations, wind speeds and sea-ice cover. Unfortunately, this approach is limited for the PMEL data, because a significant number of DMS observations are reported without corresponding wind-speed data, and no information is given on sea-ice cover. Even without matched concentration wind-speed and sea-ice data, a better estimate of sea–air flux might be attained if individual grid-cell locations were matched in time with appropriate environmental data, rather than merging climatological averages. A further limitation concerns the uncertainty in sea–air fluxes associated with the parameterization of gas exchange coefficients, particularly in ice-covered waters. Although it was initially assumed that sea-ice posed a significant barrier to air–sea gas exchange, significant DMS fluxes have been measured in ice-covered regions, likely associated with sea-ice leads.[55] Future quantitative estimates of

Southern Ocean sea–air DMS fluxes will likely improve as gas-exchange parameterisations become further refined.

2.4.2 Effects of interpolation parameters

In addition to adding a significant quantity of new primary observations to the global DMS database, our updated climatology presents an opportunity to examine the effects of algorithm parameters on the interpolation of sparse data to large oceanic regions. Two variables influence the final form of the Barnes interpolation: the data cut-off filter above which observations are discounted, and the radius of interpolation. In both instances, we believe that a significant departure from the global approach is necessary to capture regional Southern Ocean features. The Barnes interpolation[40] is based on the presumption that the value of a given variable is relatively homogeneous within the radius of interpolation. A radius of 555 km, as employed by L11, is useful for interpolating over large areas in a sparse data set, but is only valid to the extent that the underlying data field does not have small-scale spatial variability. Where significant heterogeneity exists, the interpolation field may cross distinct biogeochemical regimes with distinct DMS concentrations. Such small-scale heterogeneity appears to be particularly important in several Southern Ocean regions. Indeed, previous work [29] has demonstrated de-correlation length scales for DMS (and other biogeochemical variables) in the Ross Sea significantly less than 100 km. For this reason, we believe that the use of 555-km interpolation radius is not justified for a regional analysis of Southern Ocean DMS data, creating a visually appealing but somewhat misleading product. Our adjustment of the radius of interpolation (to 140 km) results in a climatology that more closely follows the underlying data distribution, while assigning the first-guess value to a larger number of grid cells with no nearby

primary data.

Although the radius of interpolation largely determines the spatial smoothing of the resulting climatology, the selection of a data cut-off value (either 142 or 320 nM) only affects the interpolation near the Antarctic coast, because all values over 142 nM occur in province 54 (Table 2.2). A comparison of climatologies made with the two cut-offs (Fig. 2.7) shows localised increases in the Ross and Amundsen Seas when a higher cut-off is used, but no change in the overall spatial patterns. Thus, although the use of a higher cut-off value may be important to capture local features in areas of naturally high DMS concentrations (coastal Antarctic seas), it is important to note that this does not drastically affect the overall climatology.

2.4.3 Towards a predictive algorithm for S. Ocean DMS concentrations

We attempted to correlate the updated Southern Ocean DMS data with a range of ancillary variables (Table 2.2), and also to construct an empirical predictive model using a stepwise linear regression. The lack of any strong pair-wise correlation coefficients (Table 2.2) is consistent with that observed by Kettle et al. [3] and L11, but contrasts with previous studies where stronger correlations have been observed. For example, Vallina and Simo[49] have observed significant relationships between surface-water DMS concentrations and SRD, whereas Simo and Dachs[56] have reported a strong correlation between DMS and the chl *a* /MLD ratio. Although we are unable to empirically explain a significant fraction of the DMS variability across the Southern Ocean, the (weak) correlations that we did observe are consistent with some a priori expectations. For example, the positive correlation between sea-ice cover and DMS may reflect the presence of high DMS concentrations in polynya waters and marginal ice zones.[29,57] Moreover, the negative (positive) correlation between DMS and MLD (chl *a*

/MLD) is consistent with previously reported relationships.[56]

Several potential explanations exist for the poor correlations between DMS and other ancillary variables. First, although high phytoplankton biomass (approximated by chl *a*) is known to play a significant role in driving surface-water DMS accumulation, the taxonomic composition of the phytoplankton assemblages is also critical. Several studies in the Ross Sea and other Antarctic waters have consistently shown high DMS concentrations associated with blooms of the colonial haptophyte *Phaeocystis antarctica*, with lower DMS concentrations observed in diatom-dominated blooms.[29,30,57] At present, our knowledge of the large-scale spatial and temporal distributions of various phytoplankton groups in the Southern Ocean is rudimentary at best. The PHYSAT satellite algorithm[48] was developed to address this issue, providing an estimate of large-scale taxonomic distributions. In our analysis, we found a weak negative correlation between the predicted PHYSAT abundance of *Phaeocystis*-like groups, which is contrary to expectations given the observations of high DMS levels in *Phaeocystis*-dominated regions.[29,57] This result likely reflects uncertainty in the PHYSAT algorithm for Southern Ocean waters, where very few validation samples are currently available (S. Alvain, pers. comm.). Indeed, the PHYSAT algorithm does not show any *Phaeocystis*-like signatures in the Amundsen Sea polynyas even though the high DMS concentrations reported in this region were associated with a large ($>35 \text{ mg L}^{-1}$ chl *a*) *Phaeocystis* bloom.[30] Additional calibration of the PHYSAT algorithm, and the development of other remote-sensing approaches for phytoplankton taxonomic identification, will be important for future studies.

Physiological factors could also influence DMS production in surface waters, complicating the relationship between DMS concentrations and total phytoplankton biomass (chl *a*). Iron limitation is known to exert a significant influence on phytoplankton productivity over

large regions of the Southern Ocean,[24] and has been implicated as a driving force for elevated DMS and DMSP production.[7] In order to examine the potential relationship between iron limitation and DMS accumulation, we examined the spatial patterns of sun-induced chl *a* fluorescence yields (ϕ FLR). High ϕ FLR has been suggested as an indicator of phytoplankton iron limitation in Southern Ocean surface waters,[47] although rigorous validation of this interpretation remains lacking. As shown in Table 2.2, however, ϕ FLR showed no appreciable correlation with surface DMS concentrations. Several factors may explain this result. First, as a recent data product, it remains unclear exactly which factors may influence ϕ FLR. Indeed, much of the variability in ϕ FLR appears to result from surface-water irradiance levels and sea surface temperature (SST), with only a small residual component potentially attributable to iron limitation. [45-47] Even assuming that ϕ FLR does represent a true measure of iron limitation, the use of a static climatological value (averaged between December and February) cannot accurately represent temporal variability in iron limitation. The importance of using temporally resolved data is developed further below.

Based on the results of our statistical analysis, we thus conclude that there is not likely a single predictive algorithm for Southern Ocean DMS concentrations or air–sea fluxes based on satellite-derived ancillary variables. As a result, prognostic models (e.g. Gabric et al., [19] Vezina[20] and Bopp et al.[58]), will remain an important tool in predicting Southern Ocean DMS distributions and their potential responses to climate-dependent perturbations. These models can be used to derive DMS concentrations from a variety of primary forcing functions (e.g. nutrient concentrations, wind speeds, mixed-layer depths), while also representing the more complex microbial production and consumption pathways that play an important role in controlling surface-ocean DMS dynamics.

2.4.4 Temporal Variability

An average seasonal climatology necessarily presents a static picture, without capturing temporal variability. However, DMS concentrations are dependent on a complex interplay of physical and biological factors, and can vary strongly over a range of temporal scales (hours to months). The climatology can thus only capture general trends and persistent hot-spots, with limited predictive power in any given location in time and space. The revised climatology represents several new regional DMS hotspots. Some of these, including the high DMS concentrations in *Phaeocystis*-dominated waters of the Amundsen Sea polynya, [59–61] are likely to be persistent summertime features, given the very high productivity of this region, as inferred from long term satellite observations.[62] Other new features in the updated climatology, such as the high DMS waters of the Antarctic Circumpolar Current (ACC) south of New Zealand are somewhat unexpected given their location in the off-shore pelagic realm. However, as shown in Fig. 2.1, this feature is located in the vicinity of a prominent hydrographic front (southern boundary of the ACC), and examination of the monthly chl *a* climatology (Fig. 4) shows persistently elevated phytoplankton biomass in this region. In general, previous studies have demonstrated elevated phytoplankton biomass and DMS concentrations in such frontal regions.[63-65] High DMS levels in off-shore pelagic waters may thus be more prevalent than previously believed, and future surveys should focus on mapping the spatial extent and temporal dynamics of these DMS hot-spots across various Southern Ocean regions. A key objective of this future work should be a more comprehensive representation of monthly DMS dynamics in large-scale climatological fields, and examination of DMS distributions across the various Southern Ocean frontal zones.

2.5 Conclusion

The assimilation of significant new DMS observations into an updated Southern Ocean summer climatology suggests that the current global DMS climatology underestimates sea-surface concentrations and sea-air fluxes in several regions. The apparent increase in DMS concentrations and fluxes results from greater data coverage in previously under-sampled high latitude waters, and the identification of several new DMS hotspots. The methodology we used in constructing the updated climatology demonstrates the importance of using regionally appropriate interpolation parameters and data cut-off values, and demonstrates potential biases introduced by applying a global objective analysis to the Southern Ocean.

The recent advent of easily deployable, high-frequency measurement devices[27,28] has greatly facilitated the collection of oceanic DMS data. As these analytical systems become more widespread, it should be possible to incorporate autonomous DMS measurements into more routine oceanographic surveys, including ship of opportunity programs. In the latter respect, the DMS research community can take inspiration from the large database of surface ocean CO₂ measurements that has been amassed over the past two decades through the widespread deployment of ship-based underway measurement systems.[66] Moving forward, it will be important to fill in key observational gaps – most notably in the south Indian Ocean, and to quantify the spatial extent and temporal dynamics of recently identified DMS hot-spots. In addition, it may be useful to develop a more refined description of various biogeographic provinces (e.g. Arrigo et al. [58]), which may more accurately reflect regional differences in underlying DMS dynamics. Undoubtedly, the global database of DMS measurements will expand significantly over the coming decade, and we hope that our work will help guide the

assimilation of new observations into robust climatologies that can provide insight into potential climate-dependent changes in surface-ocean DMS concentrations and sea–air fluxes.

Acknowledgements

Severine Alvain and Yannick Huot provided assistance with the extraction and interpretation of PHYSAT and fFLR data respectively. Anoop Mahajan provided helpful discussions during the preparation of the manuscript, as well as access to MATLAB codes written by Arancha Lana for the L11 DMS climatology. Unpublished DMS data were obtained from deployment of the University of British Columbia MIMS system, operated by Laughlin Barker and Casey Smith on the N. B. Palmer, and by Chris Payne and Constance Couture on the Polarstern.

Chapter 2 Tables

Province ID and name	PMEL data	PMEL + MIMS data	New grid cells
51 – SSTC	126	132	6
52 – SANT	495	551	56
53 – ANTA	721	1152	431
54 – APLR	627	871	244
Total	1969	2706	737

Table 2.1 Data coverage (number of 1318 grid cells containing observations) for the original and updated data. Province names and numbers are taken from Longhurst.[26] The provinces are: SSTC, southern Subtropical Convergence; SANT, Subantarctic Water Ring; ANTA, Antarctic; APLR, Austral Polar). PMEL and MIMS respectively refer to the Pacific Marine Environmental Laboratory existing climatology and the high resolution data obtained by membrane inlet mass spectrometry.

Variable	Correlation Coefficient
Ice cover	0.34
MLD	-0.25
Chl <i>a</i> : MLD	0.24
Chlorophyll-a	0.23
SST	-0.22
% Phaeocystis	-0.20
% nanoflagellate	-0.12
FLR	0.05
NO ₃ ⁻	0.04
Salinity	0.01
Solar radiation dose	<0.01

Table 2.2 Pearson correlation coefficients relating log-transformed dimethylsulfide (DMS) abundance to other oceanographic variables. Abbreviations are: MLD, mixed layer depth; chl *a*, chlorophyll-a; SST, sea surface temperature; FLR, chl *a* fluorescence, NO₃⁻, surface nitrate concentrations

Chapter 2 Figures

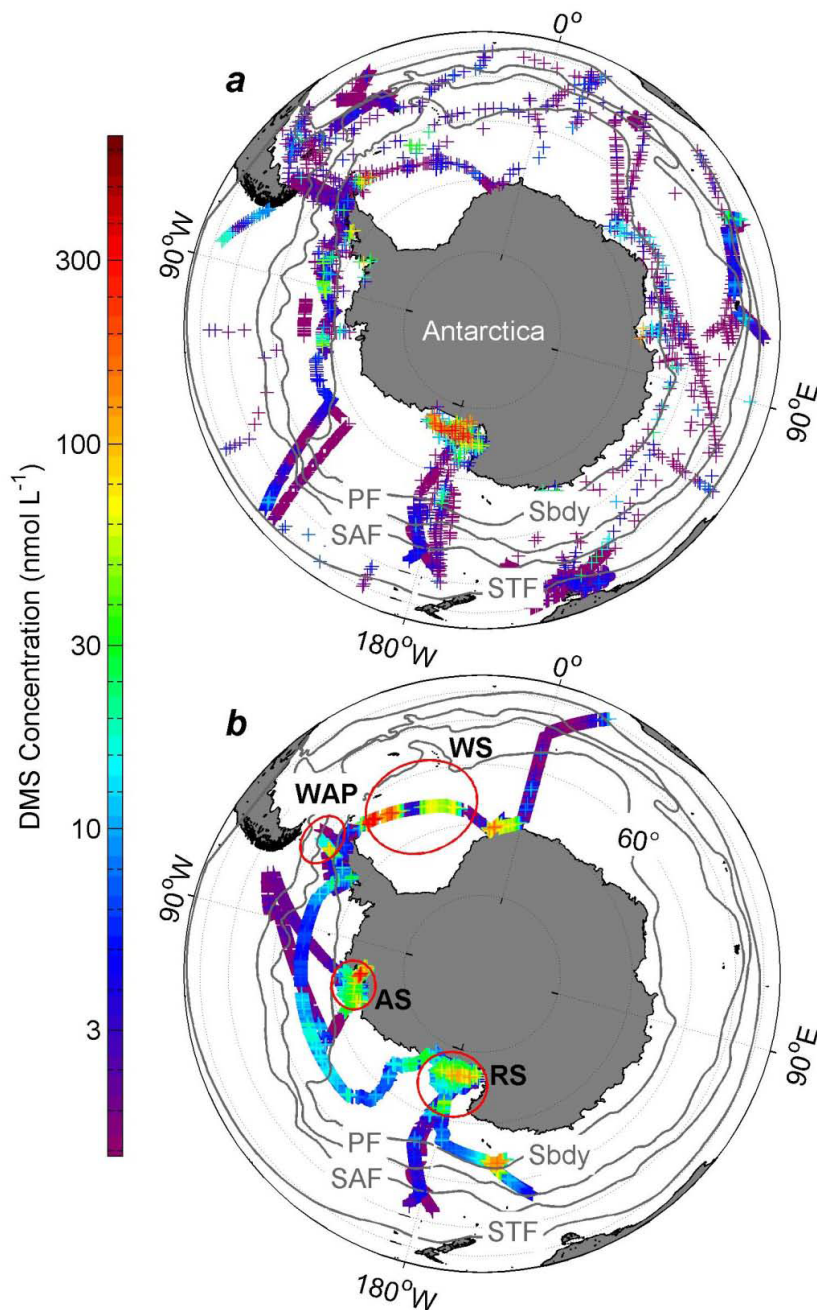


Figure 2.1 Spatial distribution of summertime Southern Ocean dimethylsulfide (DMS) measurements from the Pacific Marine Environmental Laboratory (PMEL) data (a); and MIMS surveys (b). Note the logarithmic scaling of the colour axis. Red circles denote the location of the Ross Sea (RS), Amundsen Sea (AS), West Antarctic Peninsula (WAP) and Weddell Sea (WS). Grey lines represent the mean positions of the sub-tropical front (STF), sub-Antarctic Front (SAF), Polar Front (PF) and southern boundary of the Antarctic Circumpolar Current (Sbdy). The locations of these frontal features were derived from Orsi et al.[59]

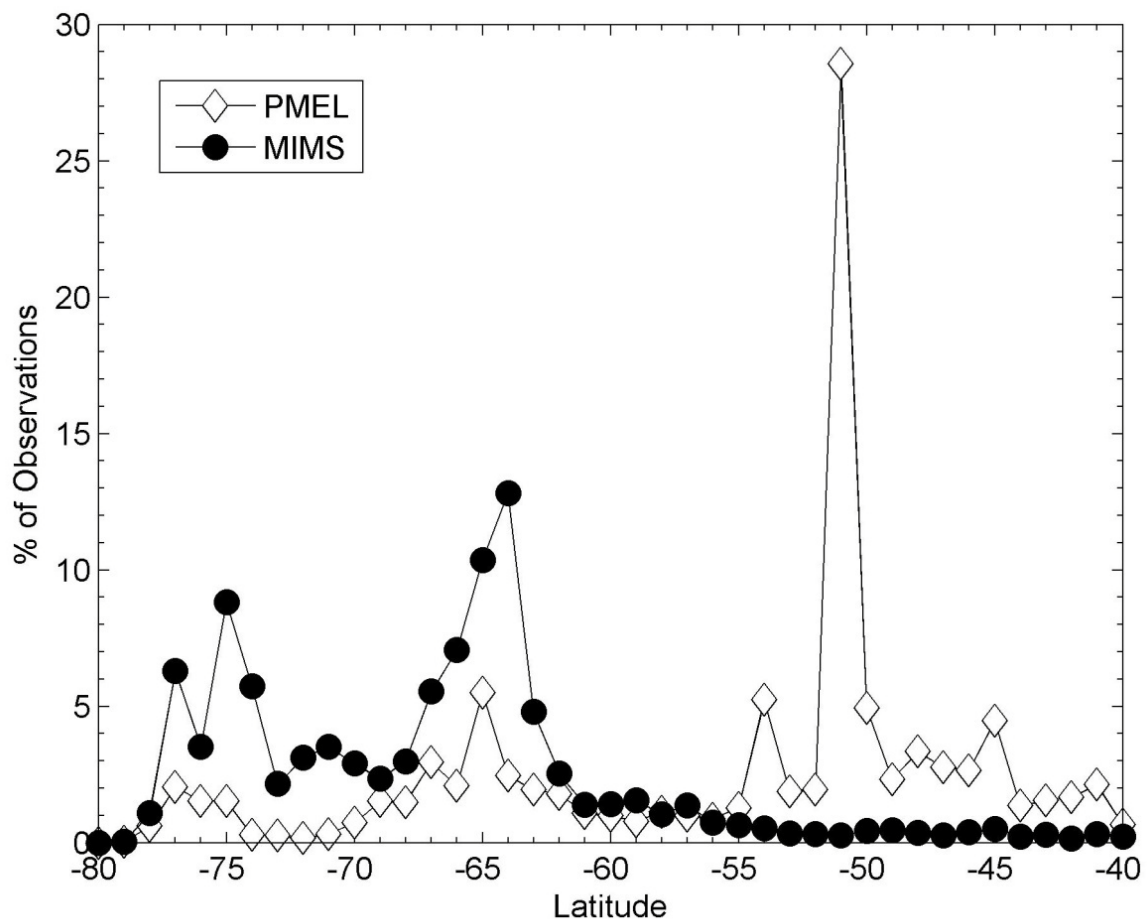


Figure 2.2 Latitudinal distribution of observations from the PMEL and MIMS data sets.

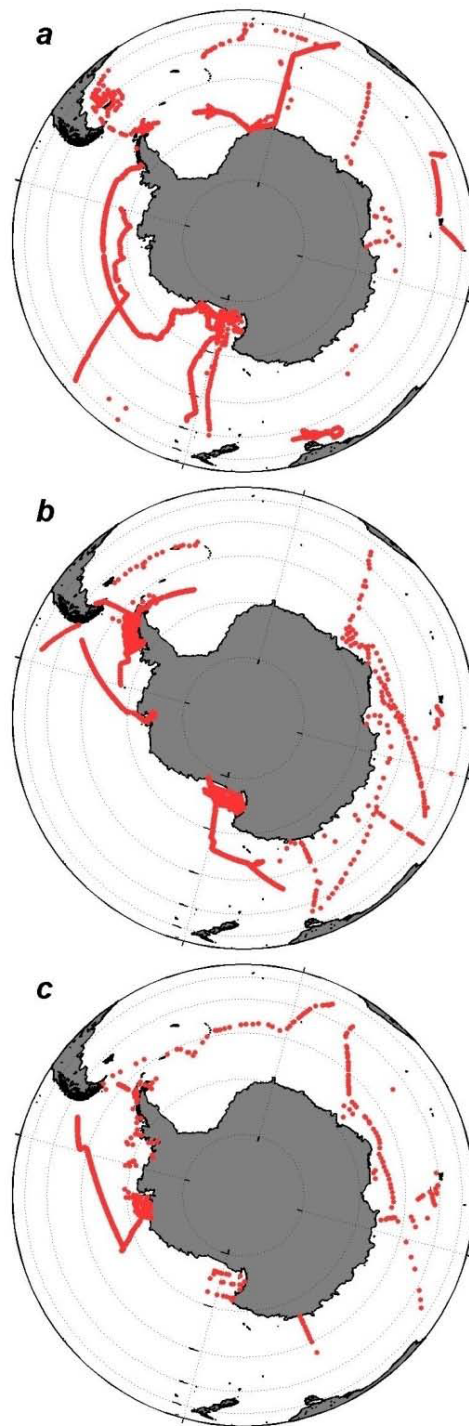


Figure 2.3 Monthly distribution of dimethylsulfide (DMS) measurements in the MIMS (a–d) and PMEL (e–h) data sets for November (a, e); December (b, f); January (c, g); and February (d, h).

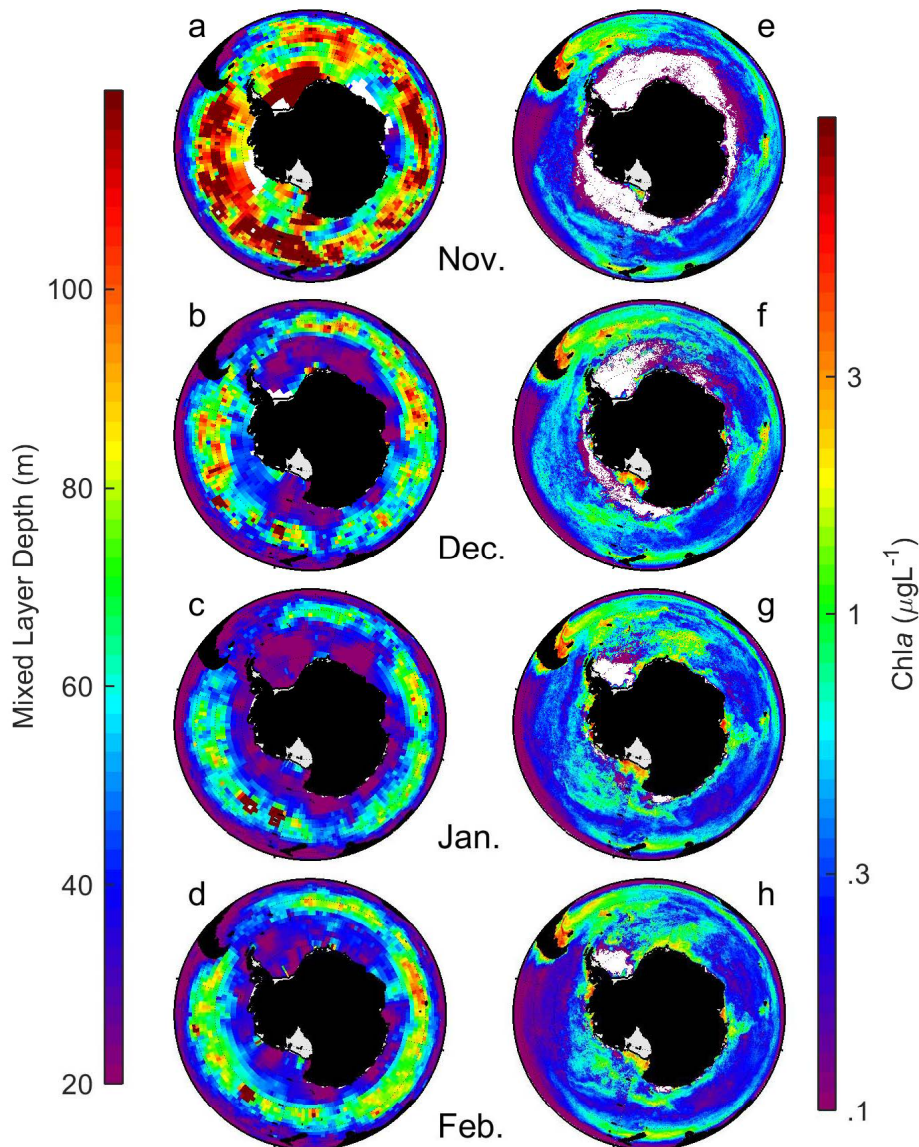


Figure 2.4 Climatological mixed-layer depths and chlorophyll-a (chl *a*) concentrations for November (a, b); December (c, d); January (e, f); and February (g, h). MLD data were taken from the IFREMER/LOS mixed-layer depth climatology (www.ifremer.fr/cerweb/deboyer/mld), and chl *a* data were taken from AquaModis 2003–13 monthly composite product (<http://oceancolor.gsfc.nasa.gov/cgi/l3>). White areas in the chl *a* distribution maps correspond to persistent sea-ice cover.

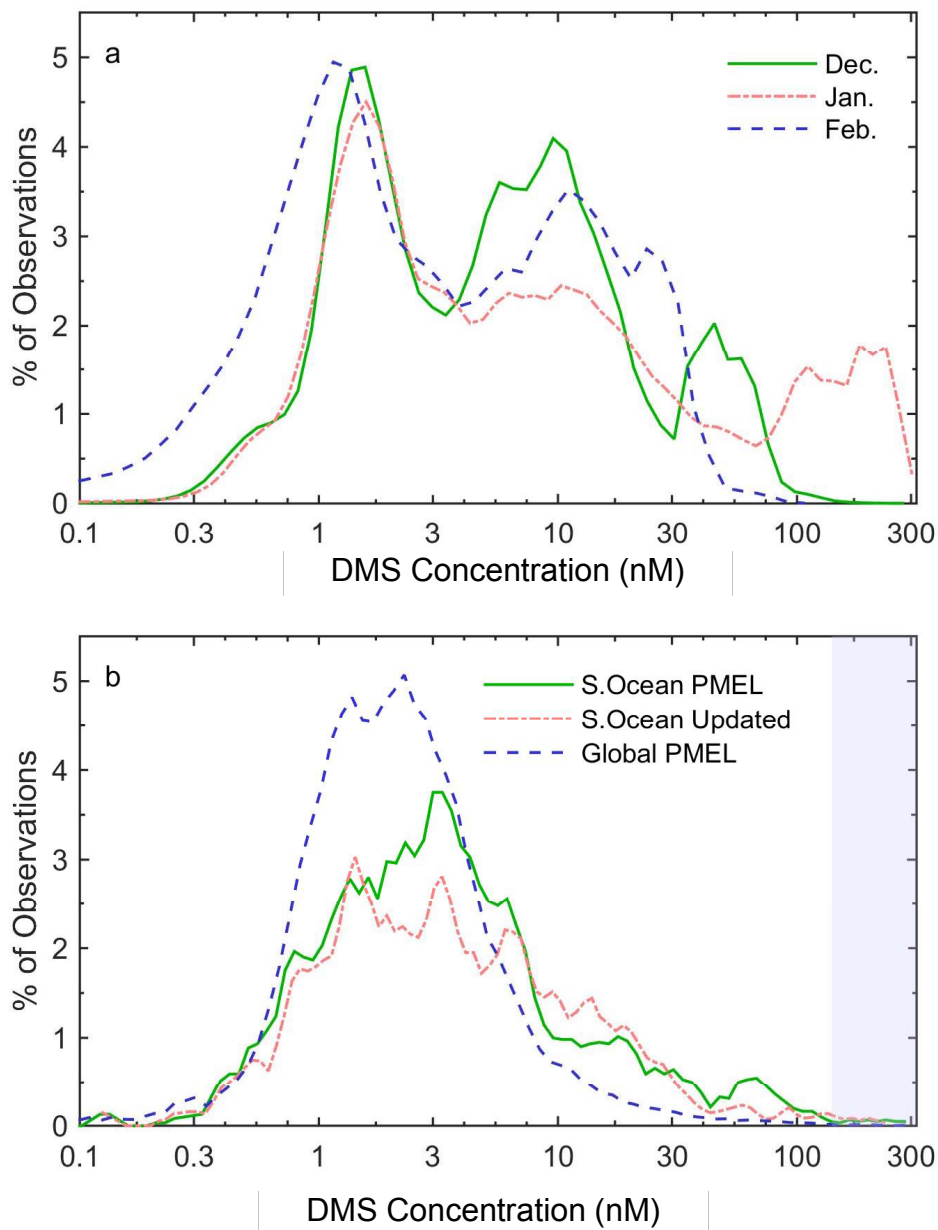


Figure 2.5 Relative frequency distribution of dimethylsulfide (DMS) concentrations for the combined PMEL and MIMS data set. Panel (a) shows frequency distributions for monthly data (December, January and February). To remove sampling biases due to the high frequency of MIMS measurements, data are shown as $1 \times 1^\circ$ binned averages. Relative frequency (percentage) is computed by normalising the number of data points in each frequency bin to the cumulative number of all observations. Panel (b) shows the frequency distribution of averaged summer data (December, January and February) for the PMEL and combined (PMEL + MIMS) Southern Ocean AQ6 data. The global PMEL data are also shown for comparative purposes.

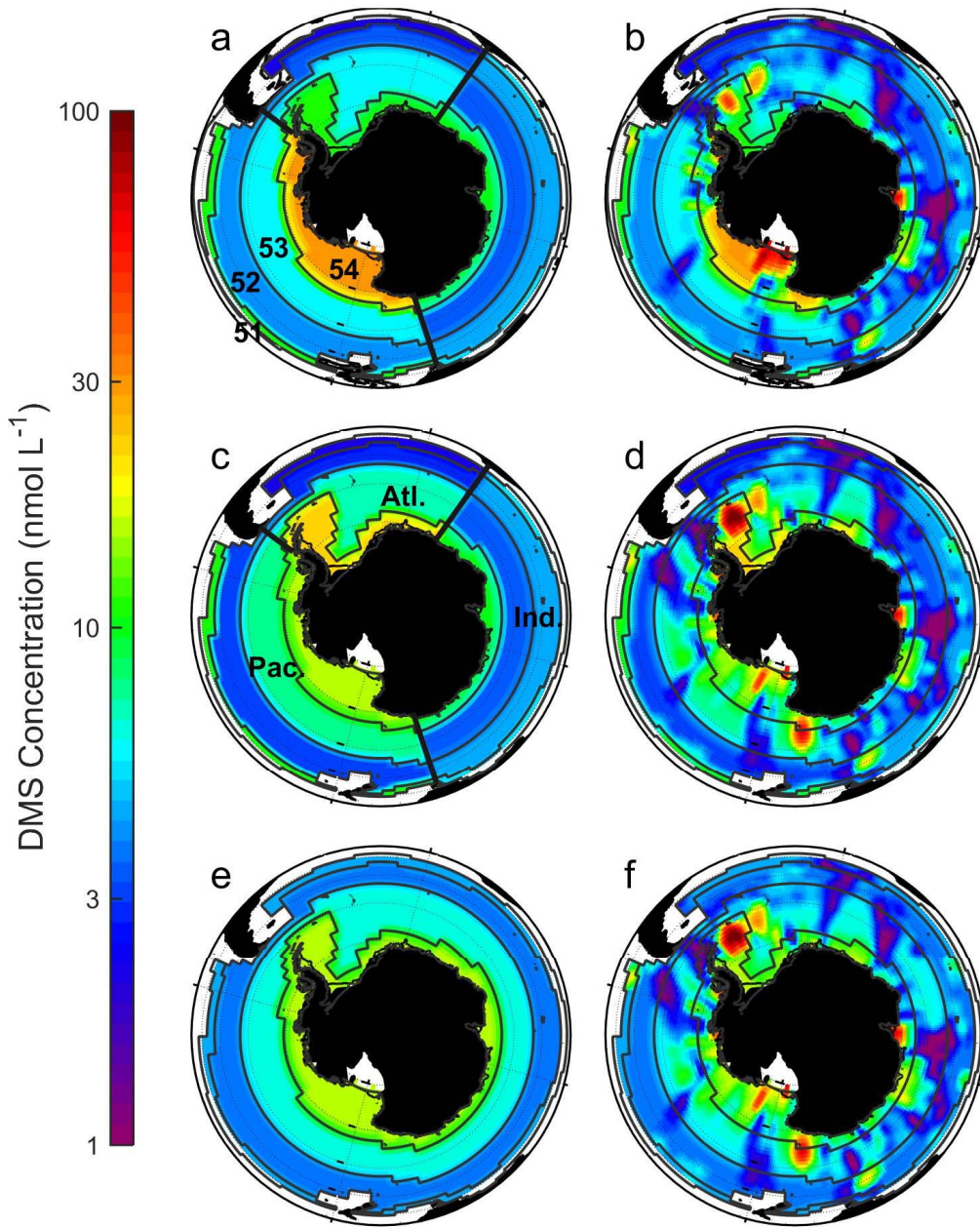


Figure 2.6 Comparison of surface dimethylsulfide (DMS) climatologies derived from the PMEL data and the updated (i.e. PMEL + MIMS) data set. (a) and (b) show the first-guess fields and resulting climatology for the PMEL data alone, whereas (c) and (d) show the results obtained using the updated data set. These maps were derived using basin-specific first-guess fields. Black lines and numbers correspond to the Longhurst ecological provinces,[29] as described in the text. (e) and (f) show the first-guess fields and resulting climatologies derived from data averaged across all three Southern Ocean basins.

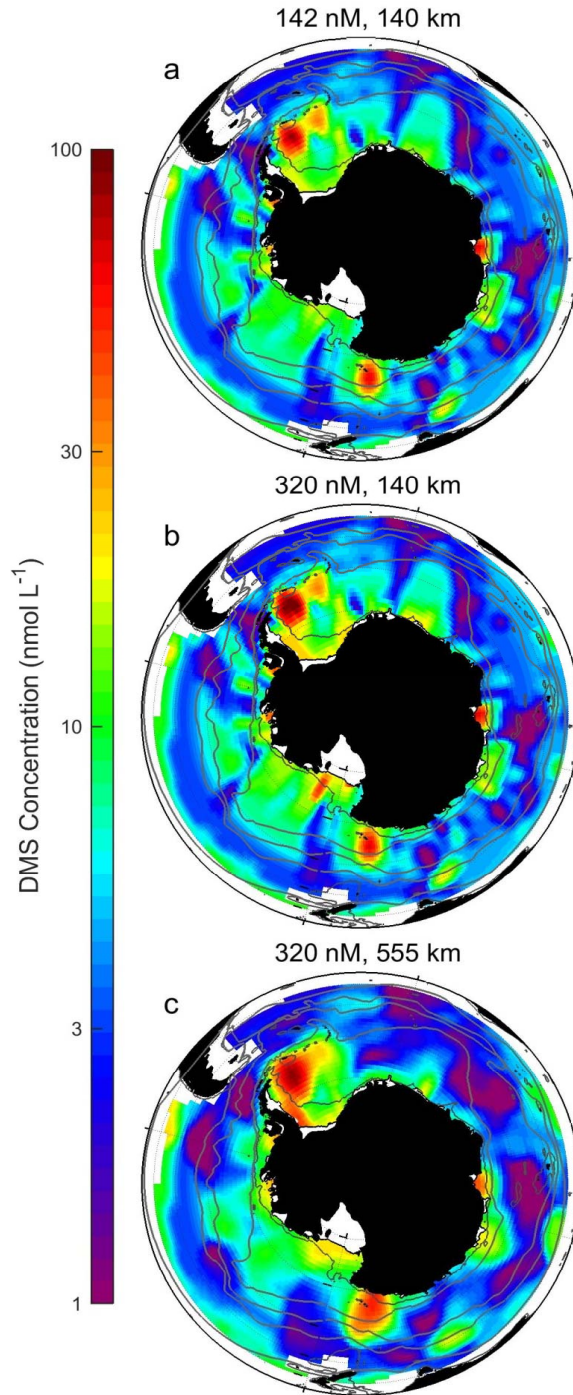


Figure 2.7 Effects of varying interpolation radius and data cut-off on surface dimethylsulfide (DMS) climatologies. (a) and (b) show the climatology derived with an interpolation radius of 140 km and data cut-offs of 142 and 320 nM respectively. Panel (c) shows the climatology derived with an interpolation radius of 555 km, and a cut-off of 320 nM. All climatologies were produced with the updated (MIMS + PMEL) data.

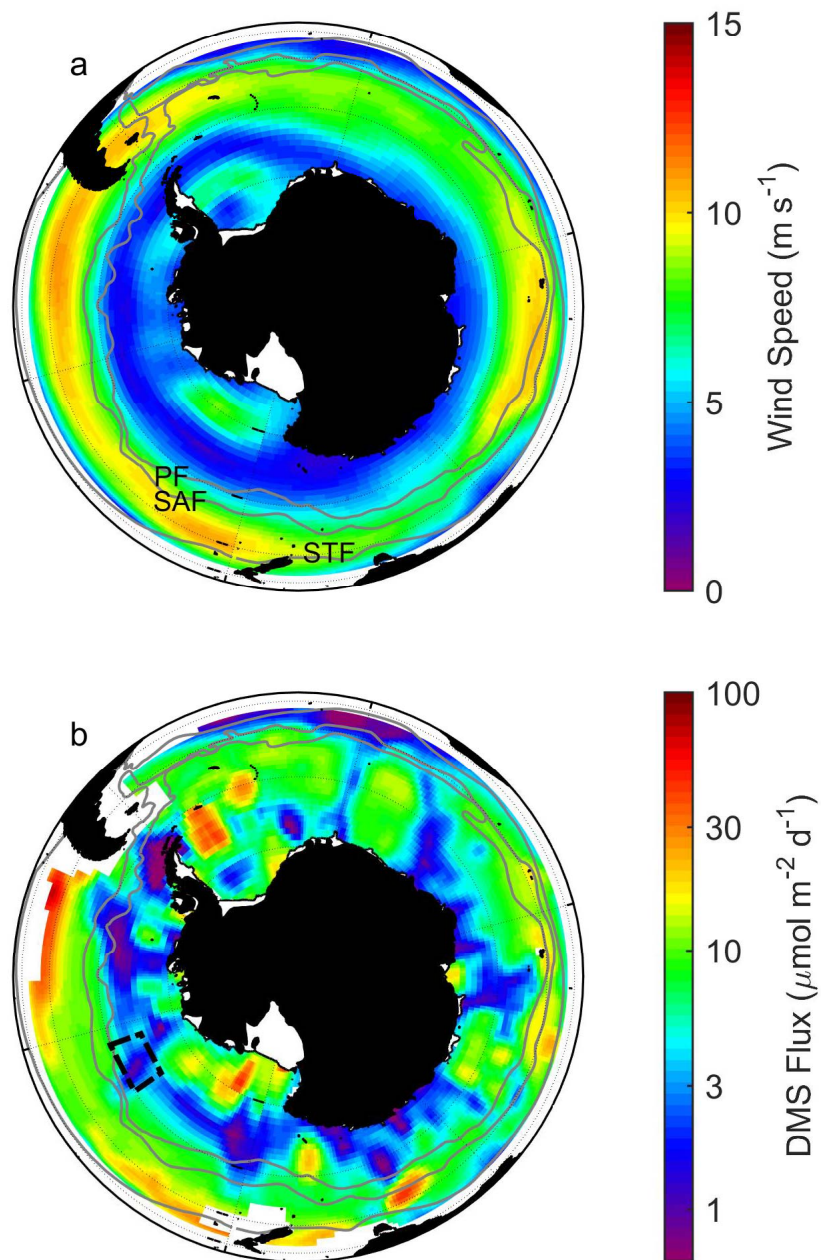


Figure 2.8 Climatological wind speeds (a); and derived dimethylsulfide (DMS) sea-air fluxes (b) for the Southern Ocean. See text for details of data sources and calculations. Black box in panel (b) represents the areas for which sea-air DMS fluxes were reported by Preunkert et al.[44]

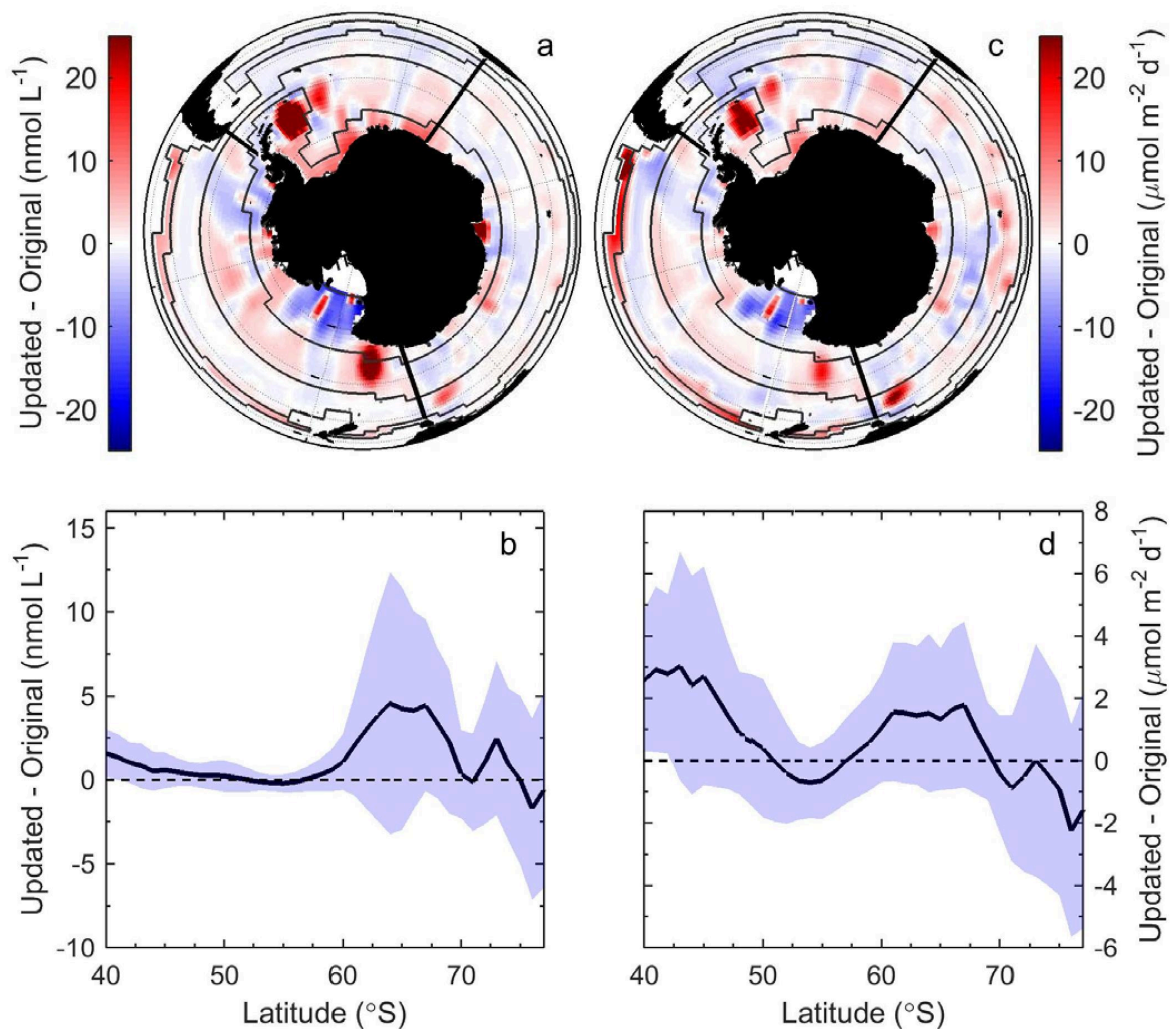


Figure 2.9 Mean difference in dimethylsulfide (DMS) concentrations and sea–air fluxes between the updated climatology and that produced by L11 (available at http://www.bodc.ac.uk/solas_integration/implementation_products/group1/dms/). (a) and (c) represent 1x1 ° spatial maps of the differences, whereas (b) and (d) show mean differences (thick black line) and standard deviation (shaded patch) across 18 latitudinal bands.

Chapter 3: The distribution of methylated sulphur compounds, dimethylsulfide (DMS) and DMSP, in Canadian Arctic Waters

3.1 Introduction

The trace gas dimethylsulfide (DMS), a degradation product of the algal metabolite dimethylsulfoniopropionate (DMSP), is the largest natural source of sulphur to the atmosphere, accounting for up to 80% of global biogenic sulphur emissions. Once in the atmosphere, DMS is rapidly oxidized to sulphate aerosols that act as cloud condensation nuclei (CCN), backscattering incoming radiation, increasing the albedo of low-altitude clouds and potentially cooling the Earth. A seminal hypothesis proposed by Charlson et al (CLAW) suggests that this negative radiative forcing will have cascading effects on marine primary productivity, leading to a DMS-mediated climate feedback loop [4]. Since its publication in 1987, the CLAW hypothesis has provided motivation for the widespread measurement of DMS in the global ocean.

3.1.1 Biological roles for DMS/O/P

Beyond their potential role in regional climate forcing, reduced sulphur compounds (DMS, DMSP and dimethylsulfoxide (DMSO)) also play critical ecological roles in the water column, where they influence microbial metabolism and food-web dynamics (for a complete overview, see Stefels 2007 [10]). DMSP, which is the biological precursor of DMS, is believed to serve numerous physiological functions in phytoplankton, with suggested roles as an osmolyte, an anti-oxidant, and a cryoprotectant under different environmental conditions. Sunda et al. (2002) suggested that oxidative stressors, such as high solar radiation or iron limitation,

may stimulate DMSP production in certain phytoplankton species [7]. DMSP production is largely species-dependent, and can vary by three orders of magnitude between phytoplankton groups, with the highest intracellular concentrations typically reported in dinoflagellates, prymnesiophytes, and haptophytes, and lower concentrations in diatoms [6].

After synthesis, DMSP can be cleaved to DMS and acrylate within algal cells, or by heterotrophic bacteria acting on the dissolved DMSP pool in the water column (DMSPd) [8]. The release of DMSP into the water column is believed to be attributable to stressed or senescent phytoplankton cells [67], and can be stimulated by zooplankton grazing and viral lysis [8]. Bacteria can also utilize dissolved DMSP as a sulphur source for protein synthesis [68], but this pathway does not lead to DMS release. The DMS yield of bacterial DMSP metabolism (i.e. the fraction of consumed DMSP that is converted to DMS) varies significantly, and may be influenced by the relative supply and demand of reduced sulfur and carbon for bacterial growth [6].

3.1.2 DMS/O/P in polar environments

Modeling studies have suggested that DMS emissions could exert an especially significant influence on regional climate in polar regions, due to the low background concentrations of atmospheric aerosols in these high latitude regions [69]. In support of this, direct observational evidence has demonstrated a link between particle formation events in the Arctic atmosphere and sea surface DMS emissions [70], motivating further quantification of marine DMS emissions in Arctic regions. Yet, logistical constraints have limited the measurement of surface water properties in many high latitude regions, and these areas remain relatively sparsely sampled for DMS/P/O concentrations. Indeed, of the approximately 48,000

data points in the global Pacific Marine Environmental Laboratory (PMEL) database of oceanic DMS measurements (<http://saga.pmel.noaa.gov/dms/>) only 5% have been made in either Arctic or Antarctic waters (~ 1600 and 1000 data points, respectively).

Despite the relatively limited sulphur observations in polar waters, an examination of the available data reveals large differences in the water column DMS distributions of the Arctic and Antarctic regions. While the summertime mean DMS concentration in the Arctic Ocean is 3.0 nM (close to the global mean value of 4.2 nM,[1]), the mean summertime DMS concentration in the Southern Ocean is ~ 3 times higher at 9.3 nM. Moreover, several areas of extraordinarily high DMS concentrations (>100 nM) have been observed in various regions of the Southern Ocean, whereas no study to date has observed DMS concentrations above 20 nM in Arctic waters. The available data thus suggest contrasting dynamics of DMS/P production in the two polar regions (i.e. Arctic vs. Antarctic).

Although Arctic and Antarctic regions share several key physical characteristics, most notably strong seasonal cycles in sea ice cover and solar irradiance, there are some critical differences. Much of the pelagic Southern Ocean is an iron-limited, high nutrient low chlorophyll (HNLC) regime, with strong seasonal changes in mixed layer depths. Low iron conditions, and seasonally-variable mixed layer light levels may induce oxidative stress and thus promote high DMS production [7]. In addition, parts of the Southern Ocean are characterized by extremely high biomass (> 30 $\mu\text{g chl } a \text{ L}^{-1}$) of *Phaeocystis antarctica*, a colonial haptophyte that is a prodigious producer of DMSP and DMS. By comparison, the highly stratified surface waters of the Arctic Ocean are believed to be primarily limited by macronutrients (i.e. nitrate), with a maximum phytoplankton biomass that is at least an order of magnitude lower than that observed in the Southern Ocean. Despite the relatively low phytoplankton biomass in Arctic

marine waters, reasonably high summertime DMS levels (max ~ 20nM) have been observed in these systems, possibly as a result of light-induced oxidative stress in salinity stratified mixed layers. It is also important to note that significant Arctic phytoplankton biomass and primary productivity may occur in sub-surface layers, and in under-ice blooms ([71]). However, the quantitative significance of these blooms for DMS production is not clear at present.

3.1.3 Arctic DMS emissions in a changing Arctic

Quantifying the DMS/O/P distribution of the Arctic Ocean is particularly important in light of the rapidly changing hydrographic conditions across this region. Rapid Arctic warming over the past several decades has been associated with a significant reduction in the extent of summer sea ice, resulting in higher mixed layer irradiance levels and a longer phytoplankton growing season. Arrigo et al (2008) suggested that a three-fold increase in primary productivity can be expected if present warming and sea-ice loss continue [72]. The effects of these potential changes on DMS/O/P concentrations and cycling remain unknown, but it has been suggested that future changes in Arctic Ocean DMS emissions could modulate regional climatic patterns [73]. Indeed, modeling work has suggested that cooling associated with increased DMS production and emissions in a less ice-covered Arctic may help offset warming associated with loss of sea-ice albedo [19]. The important climactic and biological roles of reduced sulphur compounds, combined with potentially changing dynamics in warming environments, provide the motivation for a deeper understanding of the distribution and cycling of DMS and related compounds in Arctic waters.

In this article, we present a new data set of DMS and DMSP concentrations in Arctic and Subarctic waters adjacent to the Canadian continental shelf. We used a number of recent and

emerging methodological approaches to measure these compounds in a continuous ship-board fashion. In particular, we used membrane inlet mass spectrometry (MIMS) to measure DMS with extremely high spatial resolution (i.e. sub-km scale), and the recently developed Organic Sulphur Sequential Chemical Analysis Robot (OSSCAR), for automated analysis of DMS, DMSP and DMSO. Our goal was to utilize the sampling capacities of the MIMS and OSSCAR systems to make simultaneous measurements of DMS/O/P in Subarctic Atlantic and Arctic waters, in order to expand the spatial coverage of the existing DMS/O/P dataset, and identify processes leading to spatial variability in the concentrations of these compounds in polar waters.

3.2 Methods

3.2.1 Study Area

Our field study was carried out on board the *CCGS Amundsen* during Leg 2 of the 2015 GEOTRACES expedition to the Canadian Arctic, (July 10 – August 20, 2015), on a transect from Québec City, Qc., to Kugluktuk, Nunavut. Data collection commenced off the coast of Newfoundland, and included waters of the Labrador Sea, Baffin Bay and the Canadian Arctic Archipelago (Fig. 3.1).

3.2.2 Underway sampling systems

We utilized two complementary underway sampling systems to measure reduced sulphur compounds: Membrane Inlet Mass Spectrometry (MIMS; [27]) and the Organic Sulphur Sequential Chemical Analysis Robot (OSSCAR; [32]). Detailed methodological descriptions of these systems have been published elsewhere (Tortell, 2005 [27], Asher et al. 2015 [32]), and only a brief overview is given here.

3.2.2.1 OSSCAR

The OSSCAR instrument consists of an automated liquid handling / wet chemistry module that is interfaced to a custom-built purge-and-trap gas chromatography system equipped with a pulsed photometric flame detector (PFPD) for sulfur analysis. During analysis, unfiltered seawater (3 - 5 ml) from an underway supply (nominal sampling depth ~ 5 m) is drawn via automated syringe pump into a sparging chamber. DMS is then stripped out of solution, in a 50 ml min⁻¹ N₂ flow, onto a 1/8" stainless steel trap packed with carbopack and held at room temperature. Rapid electrical heating of the trap (to ~260°C), causes DMS desorption from the trap onto a capillary column (Restek SS MXT, 15m, 80 °C, 2 ml min⁻¹ N₂ flow) to chromatographically separate sulphur gasses prior to detection by the PFPD (OI Analytical, Model 5380). Light emitted during combustion in the PFPD is converted to a voltage and recorded by a custom built Labview data acquisition interface. Following the completion of DMS analysis, 5N sodium hydroxide is added to the sparging chamber for 14 minutes to cleave DMSP in solution to DMS, following the method of Dacey and Blough [74]. The resulting DMS is sparged out of solution and measured as described above. The sparging chamber is then thoroughly rinsed with Milli-Q water, and the process can be repeated. As we used unfiltered seawater for our analysis, it is important to note that our data represent total DMSP concentrations (DMSPt), which is the sum of dissolved and particulate pools.

The OSSCAR system is designed to automate the collection of seawater for sequential analysis of DMS, DMSO, and DMSP in the same sample. During our cruise, however, we experienced problems with the DMSO reductase enzyme used to convert DMSO to DMS for analysis (see [32]), and we therefore configured the instrument to run only DMS and DMSP at sea, with one cycle requiring roughly 30 minutes.

3.2.2.2 MIMS

We used Membrane Inlet Mass Spectrometry (MIMS) to obtain very high frequency measurements (~ several data points per minute) of DMS concentrations and other gases in surface seawater. Using this system, seawater from the ship's underway loop was pumped through a flow-through sampling cuvette attached, via a silicone membrane, to a quadrupole mass spectrometer (Hiden Analytical HPR-40), and DMS was measured by detecting ions with a mass to charge ratio of 62 (m/z 62) every ~30 seconds. The DMS signal was calibrated using liquid standards held in a water bath flushed with flowing surface seawater, with a constant supply of DMS from a calibrated permeation device (VICA metronics). The primary effluent from the permeation tube (held at 30 °C) was split among several capillary outflows and mixed into a N₂ stream (~ 50 ml min⁻¹) to achieve a range of DMS / N₂ mixing ratios for bubbling into standard bottles. Concentrations of DMS in the standard bottles were cross-validated by measuring discrete samples using the OSSCAR system.

3.2.3 Post-processing of DMS data

Raw data outputs (voltages) for both OSSCAR and MIMS measurements were processed into final concentrations using MATLAB scripts. For OSSCAR data, raw voltages were captured with a sampling frequency of 5 Hz. Sulfur peaks eluting off the GC column were integrated using a custom MATLAB script, with correction for baseline signal intensities. DMS concentrations were derived from peak areas using the calibration curves as described above. To quantify instrument drift, DMS concentrations measured in inline standards were smoothed with a 3-pt running mean filter, then interpolated and compared to the known standard concentration to provide a drift correction factor for every data point.

3.2.4 Ancillary seawater data

Shipboard salinity, temperature, sea ice, wind speed, and chlorophyll *a* (chl *a*) measurements were collected using several underway instruments. We used a Seabird Electronics thermosalinograph (SBE 45) for continuous surface temperature and salinity measurements, and a Wetlabs Fluorometer (WetStar) to measure chl *a* fluorescence, as a proxy for phytoplankton biomass. We note that the chl *a* fluorescence data are subject to significant diel cycles associated with light-dependent fluorescence quenching. All sensors were calibrated prior to and following the summer expedition. CTD depth profiles were used to measure vertical profiles of salinity and potential temperature, from which we computed density using the Seawater Toolbox in MATLAB. The mixed layer depth was defined as the depth where density exceeded surface values by 0.125kg m^{-3} .

3.2.5 Phytoplankton biomass and taxonomic composition

In addition to underway data, photosynthetic pigment samples were collected at a number of discrete oceanographic stations (see Table 3.3). For each station, duplicate samples (250-500 mL) for chl *a* analysis were filtered onto pre-combusted 25 mm glass fiber filters (Whatman GF/F) using low vacuum pressure (<100 mm Hg). Filters were stored at -20 °C and chl *a* was determined using fluorimetric analysis following the method of Welschmeyer (1994) [75] within a few days of sample collection. Duplicate 1-2 L samples were filtered onto pre-combusted 25 mm GF/F for pigment analysis by reverse-phase high-performance liquid chromatography (HPLC). Filters were dried with absorbent paper, flash frozen in liquid nitrogen and stored at -80 °C until analysis following the method of (Pinckney, 2013) [76]. We used several diagnostic pigments as markers for individual phytoplankton groups, as described by Coupel et al (Coupel

2015; Table 1).[77] Following HPLC pigment processing, data were interpreted with the chemotaxonomy program CHEMTAX V1.95, using the pigment ratio matrix described by Taylor et al [78].

3.2.6 DMS Sea-Air Flux

We derived sea-air fluxes of DMS from MIMS-derived DMS concentrations, as these measurements had higher resolution and spatial coverage than OSSCAR observations.

We computed sea-air flux as:

$$F_{\text{DMS}} = k_{\text{DMS}} (\text{DMS}_{\text{sw}}) (1 - A)^{0.4} \quad (1)$$

where DMS_{sw} is the concentration of DMS in the surface ocean and k_{DMS} is the gas transfer velocity derived from the equations of Nightingale et al. [42], normalized to the temperature and salinity-dependent DMS Schmidt number of Saltzman et al. [43], and A is percent sea ice cover. The scaling exponent of 0.4 accounts for the effects of sea ice on gas exchange and is derived from the work of Loose et al. [44]. Sea surface salinity and temperature measurements described in section 2.5 were used in the calculations. Wind speed data were obtained from the ship's anemometer (AAVOS data, Environment Canada), while sea ice data were from SSM/I mapped images (<http://ifremer/cersat/products/gridded/psi-concentration/data/arctic/daily/netcdf/2015/>). Sea ice percent cover along the cruise track was derived by a two dimensional interpolation of the ship's position in time and space against the daily sea ice data products.

3.3 Results

3.3.1 Oceanographic setting

Figures 3.1 and 3.2 show the distribution of hydrographic properties across our cruise survey region. Over our sampling area, surface water temperatures varied between -1.2 and 10.2 °C, while surface salinity ranged from 10.7 to 34.7 psu (Fig. 3.1c,d). The warmest and most saline waters were found in the Labrador Sea, with cold fresher waters in Hudson Strait and the Canadian Arctic Archipelago. Underway chl *a* fluorescence varied between 0.04 and 2.96 $\mu\text{g chl/L}^{-1}$, averaging 0.20 $\mu\text{g chl/L}^{-1}$. Highest chl *a* fluorescence was observed in a localized region within Baffin Bay, where we also observed a sharp temperature and salinity frontal zone (Fig 3.1e, boxed region). Mixed layer depths ranged from 5 - 50 m, and were deepest in the Labrador Sea and shallowest in the stations of the Canadian Arctic Archipelago. The cruise transect was characterized by a variable amount of sea-ice cover, ranging from fully ice-free waters in the Labrador Sea to significant ice cover in the northern Hudson Bay and parts of the Canadian Arctic Archipelago (Fig. 3.2e).

3.3.2 Observed DMS/P concentration ranges

The DMS data shown in Fig. 3.1 are derived from MIMS measurements, since these have wider geographic coverage and greater spatial resolution. The DMSP measurements (~300 data points) are derived from OSSCAR. DMS concentrations measured with MIMS ranged from 0.2 nM to 12 nM, averaging 2.7 ± 1.5 (standard deviation) nM, while DMS concentrations measured with OSSCAR ranged from 0.1 nM to 17 nM, averaging 3.2 ± 2.4 nM. DMSP concentrations measured with OSSCAR ranged from <1nM to 160 nM, averaging 30 ± 29 nM. (For greater

visual resolution, the scale of the DMS chart in Figure 3.2a and 3.3a is cut off at 12 nM – less than one percent of DMS observations were above this cutoff.)

Figure 3.3 shows the distribution of DMS/P along the cruise track. In general, we observed reasonably good coherence between DMS measurements made by MIMS and OSSCAR, with similar absolute values of data and spatial patterns. There were, however, a notable offsets in the early Aug. measurements (~ 7000 km of the cruise track, Fig. 3a), where OSSCAR DMS data were consistently higher than MIMS data. Notwithstanding this offset (for which potential reasons are addressed in the discussion), the good coherent spatial patterns in data derived from these independent methods is encouraging.

Examination of the data in Figure 3.3 reveals that high DMS concentrations were sometimes, but not always, accompanied by high DMSP concentrations. For example, a sharp increase in measured DMSP concentrations (around km 7000-7400) on the cruise track was accompanied by a sharp increase in DMS measured by both instruments, while low-DMS waters observed around km 9400 along the transect also showed very little DMSP. Over the portion of the transect where measurements of both DMS and DMSP were available, the concentrations of these compounds exhibited a positive correlation ($r = .52$, $p \ll .001$). There were, however, a number of regions where increased DMS concentrations were not always accompanied by increases in DMSP (e.g. ~ km 8000).

3.3.3 Comparison of gradients in DMS data with hydrographic features

The high sampling frequency of MIMS measurements allows the comparison of DMS observations with other underway environmental variables, and enables the quantification of small-scale DMS concentration gradients in near real-time. Figure 3.2 shows a cruise track

record of MIMS-measured DMS concentrations in relation to salinity, temperature, chlorophyll fluorescence, and ice cover. This presentation highlights a number of small-scale features in phytoplankton biomass, hydrography and DMS concentrations along the cruise track. For example, several sharp increases in DMS early in the cruise (kms 2100, 3300, and 3800, Fig 3.2a) were accompanied by strong gradients in temperature and, to a lesser extent, salinity. An increase in DMS concentrations around km 7200 in the cruise track (Fig 3.2a) was associated with a simultaneous drop in sea-surface temperature and salinity, and in close proximity to a sharp increase in chl *a* fluorescence around km 7000 in the cruise track (Fig 3.2c).. This feature is located in Baffin Bay (Fig. 3.1a-e(boxed region)). From Fig 3.3b, we see that the highest concentrations of DMSP recorded along the transect coincide with this localized region of elevated chlorophyll at km 7000. Interestingly, this area was also characterized by strong gradients in sea ice concentrations, and the low salinity waters are indicative of localized ice melt. Figures 3.1d and 3.2d also show the large-scale salinity gradients in the Hudson Bay and the Canadian Arctic Archipelago, highlighting the freshwater influx in these near-shore areas. DMS concentrations showed relatively little variability across these salinity gradients.

In order to more closely examine small-scale structure in DMS and other surface water variables, we calculated spatial gradients in the data to examine the coherence of frontal features in DMS, salinity, temperature and chl *a* fluorescence. For this analysis, we computed gradients in each oceanographic variable within a neighborhood of 100 points surrounding each point.

Gradients (G) for each variable V (DMS, SST, chl *a*, and salinity) were calculated at each point x as follows:

$$G_x = \frac{V_{x+50} - V_{x-50}}{D_{x+50} - D_{x-50}} \quad (2)$$

Here, G is gradient (in units of change per km), V is the value of the variable at a point x , and D is cruise track distance at x . A neighborhood of 100 points was subjectively chosen because it best captured the observed variability in the data, representing an intermediate value between a very localized neighborhood (eg. 10 points), which would only consider changes close to the point, and a large neighborhood (e.g. 1000 points), which would smooth the features. The resulting figure qualitatively demonstrates a coherence of DMS gradients with salinity, chlorophyll, and sea surface temperature (see grey boxes).

3.3.4 Correlation with ancillary oceanographic variables

We computed Pearson correlation coefficients of DMS and DMSP with all available underway datasets: salinity, sea surface temperature, chl a fluorescence, and ice cover. We also examined the potential relationship between DMS concentrations and MIMS-derived $p\text{CO}_2$, and $\Delta\text{O}_2/\text{Ar}$ (Tortell et al., in prep; data not shown). Because of the greater spatial coverage and higher sampling resolution of the MIMS data, we chose to use MIMS DMS concentrations (rather than OSSCAR data) to compute DMS correlations. The results can be seen in Table 3.1. Only correlations significant at a $p < .05$ level are included. A strong positive correlation ($r = .66$, $p = \ll 0.001$) was found between DMSP and underway chl a fluorescence, suggesting the presence of high DMSP-producing taxa in the phytoplankton assemblages of waters with high DMS concentrations. Over the whole transect, we observed a weak negative correlation between DMS/P and ice cover ($r = -0.26$ for DMS: ice cover and $r = -0.34$ for DMSP: ice cover, $p \ll .001$ in both cases). Interestingly, A weak positive correlation was found between DMSP/chl a and ice cover ($r = 0.52$, $p = 0.37$), suggesting potential roles for ice phytoplankton in DMSP production at the sampled stations. However, it is interesting to note that high chl a fluorescence and

DMS/P concentrations and often occurred in areas of intermediate ice cover (kms 3300, 7300, and 9200 on the cruise track, Fig 3.2e), potentially reflecting the influence of ice-edge blooms or under-ice phytoplankton assemblages. Potential mechanisms for these features are addressed in the discussion.

3.3.5 Phytoplankton taxonomic distributions

Using measurements of accessory photosynthetic pigments, we examined spatial patterns in the taxonomic composition of phytoplankton assemblages – a description of HPLC marker pigments and their associated phytoplankton taxa, adapted from Coupel 2015, is given in Table 3.2. The distribution of pigments across our sampling stations is presented in Table 3.3, along with measurements of mixed layer depth and ice cover, while CHEMTAX-derived assemblage estimates are shown in Table 3.4. We chose to normalize pigment concentrations to total chl *a* in order to correct for large potential differences in total phytoplankton biomass.

Total HPLC-measured chl *a* was relatively low throughout the study area, ranging from 0.11 to 0.56 µg/L. DMSP:chl *a* ratios measured from HPLC chl *a* data ranged from 52.31 nM /µg to 181.4 nM/µg. For the nine sampling stations that had both HPLC and DMS/P data, the strongest correlation ($r = 0.76$, $p = 0.08$) for DMSP:chl *a* was found with fucoxanthin / chl *a*, which has been used as a marker pigment for diatom species (77), and which was present in elevated quantities at all stations. Though water column diatom species are not normally associated with elevated DMSP production (6, 10), bottom-ice diatoms have been previously reported as a source of high DMS/P (79), providing a potential explanation for this phenomenon. Pigment data indicated the presence of haptophytes, dinoflagellates, and prymnesiophytes markers in varying quantities at all stations (see Table 3.3), suggesting a mixed assemblages

across our survey region. In contrast to the observed relationship between DMSP:chl *a* ratios and fucoxanthin, no significant relationships between DMS: chl *a* and any other marker pigments were found.

CHEMTAX pigment analysis shows that all stations in the study area were diatom-dominated. Weak positive correlations were found with DMSP:chl *a* ratios and several phytoplankton taxa as follows: diatoms ($r = 0.75$, $p = .088$), c3-flagellates ($r = 0.76$, $p = .082$), and dinoflagellates ($r = 0.68$, $p = 0.13$). A positive correlation with c3-flagellates and dinoflagellates is consistent with the known high concentration of intracellular DMSP in these phytoplankton groups, while a strong correlation with diatoms may point to under-ice diatoms, which have been previously shown to be strong DMS/P producers (see Introduction).

3.3.6 Comparison with the PMEL database

Figure 3.5 shows a comparison between our DMS measurements and other summertime Arctic DMS data in the PMEL database. For this comparison, only PMEL measurements made above the Arctic Circle (66.56°N) in the summer months of June-August were included, resulting in a total of 415 measurements. As shown in this figure, the majority of available summertime PMEL DMS/O/P measurements are found in the Atlantic region of the Arctic, and in the Bering Sea, with limited data in the Canadian Archipelago (for an overview of Arctic DMS/O/P studies performed to date, see Levasseur 2013).

For the visualization in Fig. 3.5a, we used DMS measurements made by OSSCAR, whereas both sets of data were included in the frequency distribution analysis (Fig. 3.5b). The results presented in Fig. 3.5 suggest that our measurements are representative of the broader Arctic context, with similar data frequency distributions (Fig. 3.5b) for all three DMS datasets

(MIMS, OSSCAR, and PMEL). Arctic DMS observations are heavily skewed towards lower values, with a large proportion of each dataset containing values less than 2 nM, and comparatively few (< 3% of all data) concentrations greater than 10 nM. From the map, we also see that our dataset spatially complements the existing summer dataset, helping to expand the spatial coverage of DMS observations in the Arctic Ocean.

3.3.7 DMS Sea-Air Flux

Figure 3.6 shows DMS sea-air flux as computed from MIMS-measured DMS seawater concentrations, wind-speed and sea-ice cover, using the parametrization described in section 2.7. DMS Sea air fluxes ranged from 0 to 80 $\mu\text{mol S m}^{-2} \text{ day}^{-1}$, with peak sea-air flux observed around km 5500 on the cruise track. Sea-air flux is highly dependent on wind-speed and sea-ice cover, with the result that even high concentrations of seawater DMS yielded low sea-air flux when low wind and/or high sea-ice was present (e.g. kms 2100, 7200, 8300). Conversely, very high sea-air fluxes were observed when moderately high DMS concentrations coincided with high wind-speeds and ice-free waters (eg. km 5400). The range of sea-air fluxes calculated was consistent with recent summertime sea-air DMS fluxes modelled in Resolute Bay (Hakase Hayashida, pers. comm.)

3.4 Discussion

Our high-resolution DMS/O/P observations provide new reduced sulphur data for an undersampled region of the Arctic Ocean, while enabling high-resolution comparison with other oceanographic parameters. Below, we focus our discussion on the observed relationship between gradients in DMS and other oceanographic variables, and on the relationship between DMSP and

phytoplankton biomass and taxonomic composition. We also compare our results to previously published measurements in the Arctic, and discuss the comparability of the two DMS measurement methods utilized. Finally, we aim to situate our results in the context of the changing hydrography and phytoplankton ecology of the Arctic Ocean.

3.4.1 Comparison with existing measurements

Our dataset complements the sparse existing spatial coverage of reduced sulphur in the Canadian Sector of the Arctic Ocean. Several past Arctic DMS/O/P water column studies are summarized in Table 3.5. This table focuses heavily on DMS/O/P measurements made in the Canadian sector and Greenland waters, serving to provide context for our measurements performed in similar environments. These data are drawn from different times of year, and from phytoplankton assemblages of varying taxonomic composition, allowing us to examine sulphur production capacity of Arctic phytoplankton in several different contexts. For example, Bouillon et al observed low DMS concentrations ($<1\text{nM}$) during a large spring diatom bloom ($\sim 15 \mu\text{g L}^{-1}\text{chl } a$) in the North Water region [80]. In contrast, higher DMS concentrations have been reported later in the season when total phytoplankton biomass is lower, and taxonomic composition has shifted towards flagellates. Working in the same geographic region as Bouillon, Motard-Cote (2012) reported higher late summer (September) DMS levels (maximum = 4.8 nM), which were accompanied by moderate chl *a* concentrations ($0.2\text{-}1 \mu\text{g/L}$ [81]), while Luce et al report very low DMS ($<1\text{nM}$) associated with moderate chl *a* concentrations ($0.2\text{-}2 \mu\text{g/L}$) in a flagellate dominated community in late fall (October-November), with DMS decreasing towards the later months [82] This suggests that DMS levels in similar phytoplankton assemblages may decrease in later months, potentially due to lower light stress and reduced primary productivity.

To date, the highest recorded Arctic water-column measurements of DMS and DMSP have been observed during mid-summer blooms of the haptophyte *Phaeocystis* at the ice edge (see Gali and Simo [83]). Our mid-season (July-August) study of similar areas shows moderately high DMS (0.5-12 nM) accompanied by relatively low chl *a* (0.11-1.06 µg/L) in a mixed community where flagellates and prymnesiophytes are present (see discussion of HPLC pigments).

Together, the available data (Table 3.5 and our measurements) are consistent with a seasonal cycle in Arctic reduced sulphur production. Early-season diatom-dominated blooms exhibit high biomass and primary productivity but low sulphur production, while mid-summer phytoplankton assemblages dominated by haptophytes and dinoflagellates have lower phytoplankton biomass but higher sulphur production. This pattern is similar to the summer-time 'DMS paradox', which has been reported in lower latitude temperate marine waters [84]. In the fall, both phytoplankton productivity and DMS/P production decrease with the onset of lower temperatures and increased ice cover. Our data fit this general scenario, representing a mixed-species assemblage with moderate biomass and sulphur production relative to that observed by other researchers in Arctic mid-summer [83,85].

3.4.2 Comparability of MIMS and OSSCAR measurements

The OSSCAR and MIMS instruments have been previously shown good agreement in measured DMS concentrations in the Subarctic Pacific Ocean [32]. Similarly, we observed relatively good agreement between the two methods (Fig 3.3) over much of our cruise track, except around km 7000, when DMS measurements measured by OSSCAR were significantly higher than those measured by MIMS. This occurred in a region where very high DMSP

measurements (often one order of magnitude higher than the DMS measurements) were also observed. If small amounts of DMS remained in the OSSCAR system after DMSP analysis, these could contribute to higher measured concentrations in the subsequent DMS analysis due to sample carry-over. Another potential cause of the higher OSSCAR DMS measurements may be due to cell breakage during the sparging process in OSSCAR. In this scenario, there is the potential for release of intracellular DMSP and DMSP lyase into solution, which would lead to artificially high measured DMS concentrations. It is not possible for us to quantify the magnitude of such a potential artefact, but we note that its magnitude would likely depend on the taxonomic composition of phytoplankton assemblages.

3.4.3 Gradients in DMS and hydrographic frontal structures

The high resolution afforded by the MIMS dataset allows for the observation of fine-scale changes in DMS concentration at the sub-kilometer scale. Figures 3.2 and 3.4 clearly demonstrate that gradients in DMS and chlorophyll fluorescence often occur simultaneously with strong gradients in temperature and salinity. This suggests a potential role for hydrographic fronts in driving changes in DMS concentrations. Several potential mechanisms may explain this phenomenon. For example, the frontal mixing of distinct water masses, driven by currents, wind, or melting ice, may introduce fresh nutrients into a low-nutrient water column, stimulating primary productivity and potentially increasing DMS/P production. This stimulation of primary productivity has been observed previously by other groups. For example, Tremblay et al showed that introduction of nutrient-rich water masses through ice ablation and upwelling led to large (2-6 fold) increases in phytoplankton primary productivity [86]. Mixing of water masses may also potentially expose water column phytoplankton to light shock or osmotic stress by mixing them

upwards in the water column or introducing an abrupt salinity gradient. Both of these factors could contribute to elevated DMSP production, given its hypothesized role as an intracellular osmolyte and anti-oxidant [7,10]. Though our data do not allow mechanistic interpretation for the underlying causes of DMS variability in surface waters, the high resolution afforded by MIMS measurements enables real-time observations of DMS gradients, which may be useful in the design of future process studies examining the driving forces for elevated DMS accumulation.

3.4.4 Phytoplankton assemblage composition and mixed layer depth

The majority of the sampled stations were characterized by very shallow mixed layer depths (MLD; Table 3.3) resulting from strong salinity-based stratification of surface waters. Light stress associated with shallow MLD may contribute to elevated DMSP:chl *a* ratios. In our dataset, the shallowest MLDs were observed at stations BB3 and CAA6 (8.2 m and 6.1 m, respectively), and these stations were also characterized by very high DMSP. Though the CHEMTAX analysis suggests that all stations in the study were diatom-dominated, the DMSP:chl *a* ratios measured in our study also reflect the presence of high-DMSP producing taxa, a phenomenon also reported by other groups. Limited HPLC station data suggest that a mixed phytoplankton assemblage was present in the study area at the time of sampling, with weak correlations between the diatom marker fucoxanthin and DMSP:chl *a* ratio. When comparing our DMSP: chl *a* ratios to other measurements, it is important to note that the two ratios are not necessarily directly comparable, as we measure DMSP_t, while many other groups give results in terms of DMSP_p, missing the dissolved fraction (DMSP_d). The dissolved DMSP pool makes up a small (though highly variable) portion of the total water column DMSP pool,

and the use of DMSPt thus likely does not have a large effect on derived DMSP:chl *a* ratios. The DMSPt : chl *a* ratios we measured across our sampling stations were broadly similar to DMSPp : chl *a* values found by Motard-Cote (15-229 nM/ μg) in the same region in September [81]. In contrast, our measured DMSP / chl *a* ratios are significantly higher than those measured by Luce (who reported a maximum value of 39 nM/ μg) [82], and Matrai et al (max. 17 nM/ μg) at diatom-dominated stations in the Barents Sea. This difference likely reflects a difference in phytoplankton assemblage composition [87].

3.4.5 The interaction of DMS/P and sea ice

The presence of sea ice acts exerts a strong control on polar phytoplankton by limiting irradiance for primary productivity in the water column. This allows high concentrations of nutrients to build up, creating favourable conditions for phytoplankton blooms upon sea-ice melt. Ice edge blooms are well-documented, and can serve as a source for reduced sulphur compounds. In a 2010 study, Gali et al found that sea ice melt drove stratification of nutrient rich surface water, triggering a sharp increase in primary productivity, with associated elevated DMS and DMSP levels [83]. Many recent studies have also examined the potential of sea ice to act as a reservoir of reduced sulphur. For example, Levasseur et al reported very high concentrations of DMS and DMSP in Arctic bottom-ice diatoms [79], and suggested that the breakup of sea ice may stimulate reduced sulphur production by triggering phytoplankton blooms and releasing accumulated sulphur into the water column.

The weak negative correlations between sea ice cover and DMS/P concentration we observed is consistent with the idea that sea ice cover limits insolation, and by extension primary productivity and DMS/O/P production. It is interesting to note, however, that several sharp

increases in DMS occurred simultaneously with the occurrence of small amounts of sea ice (<20% total cover) (Fig. 3.2, kms 3400 and 7200 on the cruise track). Limited station data also indicate high DMS/P:chl *a* ratios in areas with a comparatively high sea-ice cover, at stations BB3 and CAA6 (Table 3.3) – both stations are characterized by very low phytoplankton biomass (.11 µg/L and .20 µg/L chl *a* respectively) accompanied by particularly high DMSP: chl *a* ratios (129 nM/µg and 182 nM/µg respectively). This suggests a potential role for ice-edge effects, either through the melt-induced stimulation of reduced sulphur production in DMS/P rich phytoplankton taxa, or through the release of ice-associated DMS/P into the water column. Figure 3.2d and 3.2e shows decreased salinity in partially ice-covered areas, in particular around kms4400, 7300, and 9200. Similar trends have been reported by several groups. For instance, Matrai et al (1997) [87] reported significantly higher values of DMS and DMSP in partially ice-covered waters of the Barents Sea than in ice-free regions, while Gali(2010) [83] and Leck (1996) [85]) reported highest DMS/P values along the ice edge in their Arctic surveys.

3.4.6 DMS in a changing Arctic

The Arctic marine ecosystem is currently undergoing a dramatic warming that is expected have far-reaching impact on phytoplankton dynamics and, consequently, DMS production and sea-air fluxes. Much of the ecosystem change is driven by warming and rapidly melting sea ice, which influence mixed layer stratification, light regimes and nutrient supply (REFS). Current work suggests that sea ice loss will eventually lead to a nutrient-poor, shallow-stratified Arctic Ocean with low phytoplankton biomass [88]. Nutrient limitation may favour smaller cells, shifting diatom-dominated assemblages to communities with a strong flagellate presence, and this may, in turn, increase DMSP production and DMS emissions. A modeling

study by Gabric et al (2005) projected significant increases in DMS emissions in response to MLD shallowing and ice ablation [19]. Our observations from regions with shallow mixed layer depths and mixed phytoplankton assemblages with a strong flagellate presence, do indeed exhibit elevated DMS/P concentrations, providing some support for this prediction.

3.5 Conclusion

We present a high spatial resolution transect of reduced sulphur measurements through the Canadian sector of the Arctic Ocean and Subarctic Atlantic. We demonstrate the utility of very high-resolution DMS measurements for comparison with other oceanographic variables, and show the coherence of DMS gradients with gradients in surface hydrography (salinity and temperature). This result suggests a possible role in for oceanographic frontal features in controlling DMS production. We find elevated DMS/P values in partially ice-covered regions, suggesting that ice-edge effects may stimulate DMS/P production. We also show a weak positive relationship between DMSP:chl *a* ratios and fucoxanthin, a pigment associated with diatoms,. Our data serve to significantly expand the existing spatial coverage of reduced sulphur measurements in the Arctic, while providing a baseline for future studies in a changing marine environment. Future warming of surface waters and sea-ice melt could lead to increased concentrations and sea-air fluxes of DMS, though significantly more observations will be needed to substantiate this.

Chapter 3 Tables

Variable	DMS Correlation Coefficient	DMSP Correlation Coefficient
$\Delta O_2/Ar$	0.22	0.33
Salinity	0.35	0.34
SST	0.29	0.14
Fluorescence	0.32	0.66
pCO_2	0.16	0.12
Ice Cover	-0.26	-0.34

Table 3.1 Pearson correlation coefficients relating DMS measurements made by MIMS and DMSP measurements made by OSSCAR to other oceanographic variables. Only correlations significant at the $p < .05$ level are shown.

Pigment	Associated taxa
Chlorophyll c3	Haptophyte
Peridinin	Dinoflagellates
19'-butanoyloxyfucoxanthin	Haptophytes
Fucoxanthin	Diatoms
19'-hexanoyloxyfucoxanthin	Haptophytes, Dinoflagellates
Diadinoxanthin	Haptophytes, Dinoflagellates
Violaxanthin	Dinoflagellate
Zeaxanthin	Dinoflagellate

Table 3.2 HPLC marker pigments and their associated phytoplankton taxa – adapted from Coupel et al, 2015 [77].

Station	Lat(N)	Lon(E)	MLD(m)	% Ice Cover	DMS/ chl a	DMSP/ chl a	Chl a (µg/L)	Perid/ chl a	19'But Fuc/ chl a	Fuc/ chl a	19'HexFuc/ chl a	Diadino/ chl a	
1	K1	56.1	-53.4	18.4	<i>nd</i>	6.58	<i>nd</i>	0.505	0.043	0.077	0.184	0.156	0.056
2	LS2	60.5	-56.6	41.4	<i>nd</i>	3.39	<i>nd</i>	0.587	0.051	0.012	0.277	0.025	0.024
3	BB3	71.4	-68.6	8.2	19.7	0.04	129.35	0.115	0.049	0.011	0.278	0.051	0.087
4	BB2	72.7	-67	10.26	0	21.69	93.32	0.187	0.050	0.015	0.312	0.089	0.072
5	CAA1	74.5	-80.6	32.1	<i>nd</i>	6.93	52.31	0.560	0.015	0.018	0.239	0.023	0.042
6	CAA5	74.1	-91.5	5.3	6.61	0.00	114.68	0.159	0.078	0.017	0.326	0.020	0.051
7	CAA6	74.8	-97.5	6.1	16.43	10.59	181.71	0.207	0.054	0.021	0.401	0.015	0.058
8	CAA7	73.7	-96.5	2.1	13.3	15.56	81.33	0.130	0.109	0.066	0.335	0.057	0.146
9	VS	69.2	-100.7	8.4	8.23	10.57	<i>nd</i>	0.181	0.029	0.020	0.309	0.032	0.037

Table 3.3 Mixed layer depth, ice cover, HPLC pigment measurements and DMS/P measurements made at several stations. DMS data is taken from MIMS, while DMSP data is taken from OSSCAR. *nd*= no data.

<i>CHEMTAX-derived percentage of functional group in assemblage</i>										
	Station	Diatom	Dinoflag.	Chloro.	Prasino-3	Prasino-2	Crypto.	C-P	c3-Flag.	Hapto-7
1	K1	37	14	0	11	6	4	9	1	16
2	LS2	39	19	0	17	6	1	3	7	8
3	BB3	48	15	4	7	7	8	1	5	5
4	BB2	44	16	11	9	5	4	2	1	8
5	CAA1	47	4	0	24	15	2	2	4	2
6	CAA5	50	19	1	7	3	3	2	14	1
7	CAA6	52	16	1	7	1	3	2	17	1
8	CAA7	46	11	4	11	6	8	8	0	5
9	VS	67	8	0	9	2	3	3	6	3

Table 3.4 CHEMTAX-derived phytoplankton assemblage estimates for sampled stations. Diat. = diatoms; Dinoflag = Dinoflagellates; Chloro. = Chlorophytes; Prasino-3 = Prasinophyte type 3; Prasino-2 = Prasinophyte type 2; Crypto. = Cryptophytes; Chryso-Pelago = Chrysophytes/Pelagophytes; c3-flag. = c3-Flagellates; Hapto-7 = Haptophyte type 7.

Author	Year	Month	Region	DMS (nM)	DMSP (nM)	assemblage characteristics
Bouillon 2002	1998	April-June	North Water	0.04-6.7	0-9.53 (DMSPp)	diatom dominated assemblage
Matrai and Vernet 1997	1993	May	Barents Sea	2.8 to 25.3	6-27 (DMSPp) 4-36 (DMSPd)	includes both diatom-dominated and Phaeocystis-dominated stations
Gali and Simo 2010	2007	July	Greenland Sea	0.1 to 18.3	1.4 to 163.6	haptophyte (<i>Phaeocystis</i>) dominance
Leck and Persson 1996	1991	August- October	Greenland Sea	.04-12	--	not described
Motard-Cote 2012	2008	September	Baffin Bay North Water	0.4-5.2	5-70 (DMSPp)	not described
Luce 2011	2007	October- November	High Arctic	0.05-0.8	2- 39 (DMSPp)	flagellate dominated except for diatom-dominated Baffin Bay

Table 3.5. An overview of past Arctic DMS/O/P studies performed in the summer months, focusing on observations from the Western Hemisphere.

Chapter 3 Figures

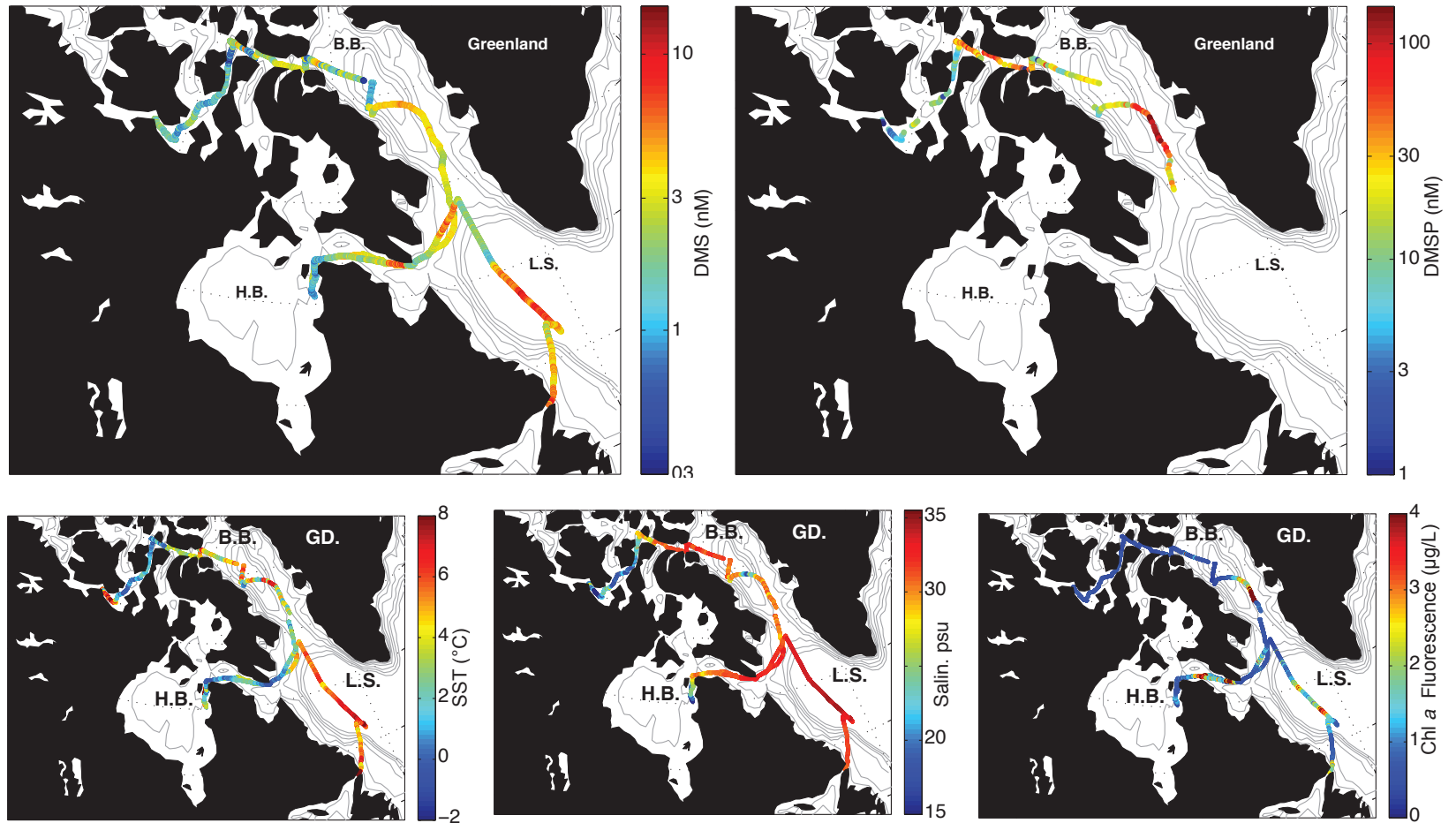


Figure 3.1 Spatial Distribution of DMS/P and Hydrographic Variables.

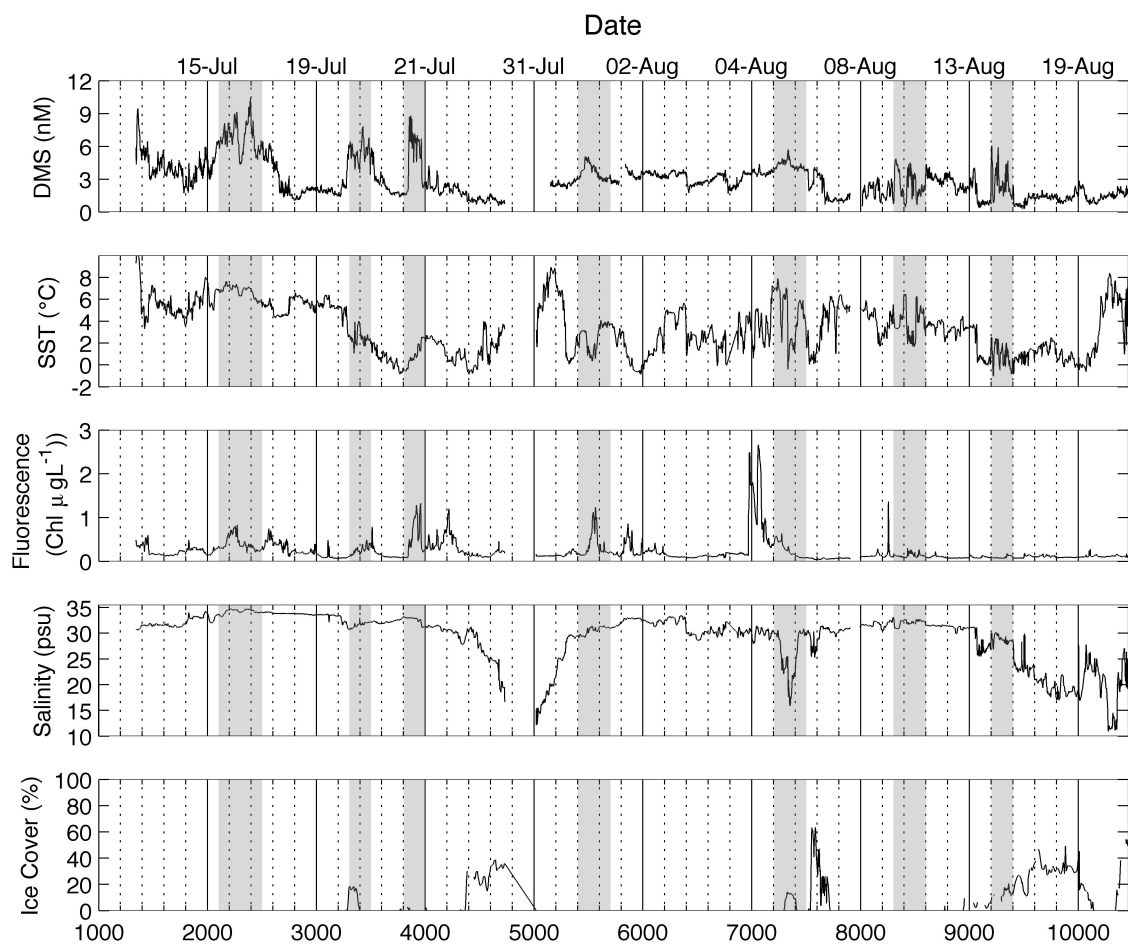


Figure 3.2 Cruise Track Record of DMS and Hydrographic Variables. Areas of high DMS concentration are shaded grey, for comparison with other hydrographic features.

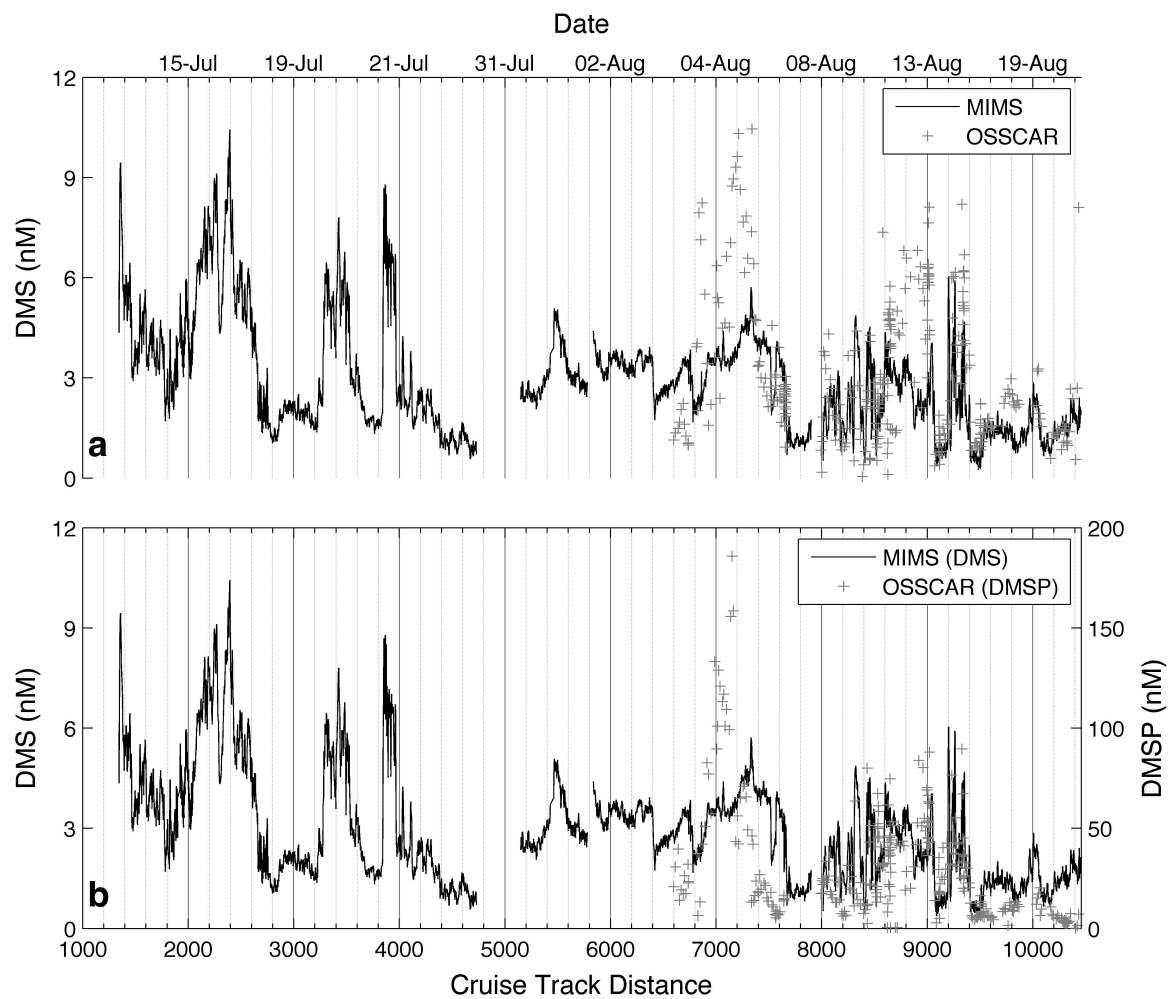


Figure 3.3 Cruise Track Record of MIMS and OSSCAR DMS/P Measurements

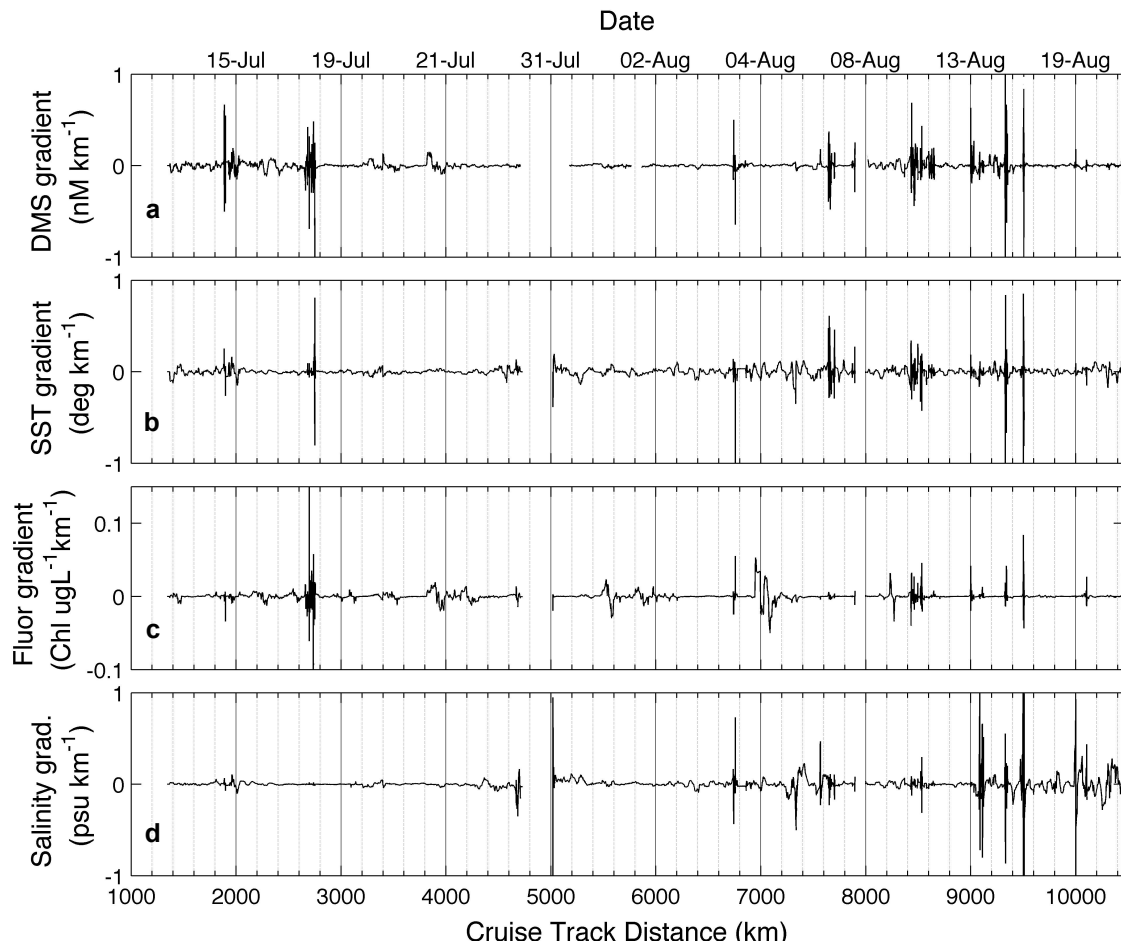


Figure 3.4. Gradients in DMS and Hydrographic Variables

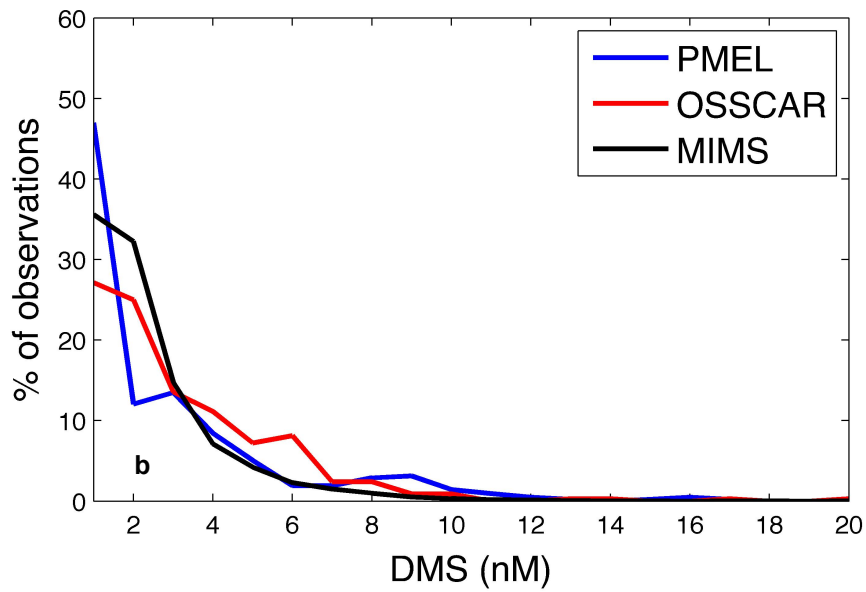
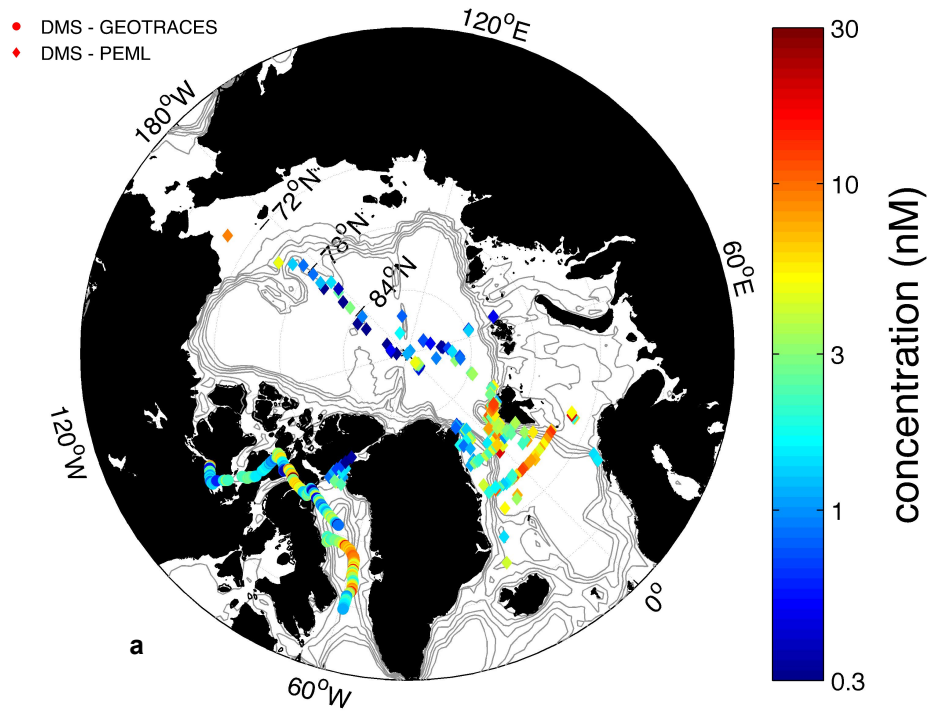


Figure 3.5. Comparison of OSSCAR-Measured DMS with PMEL Database.

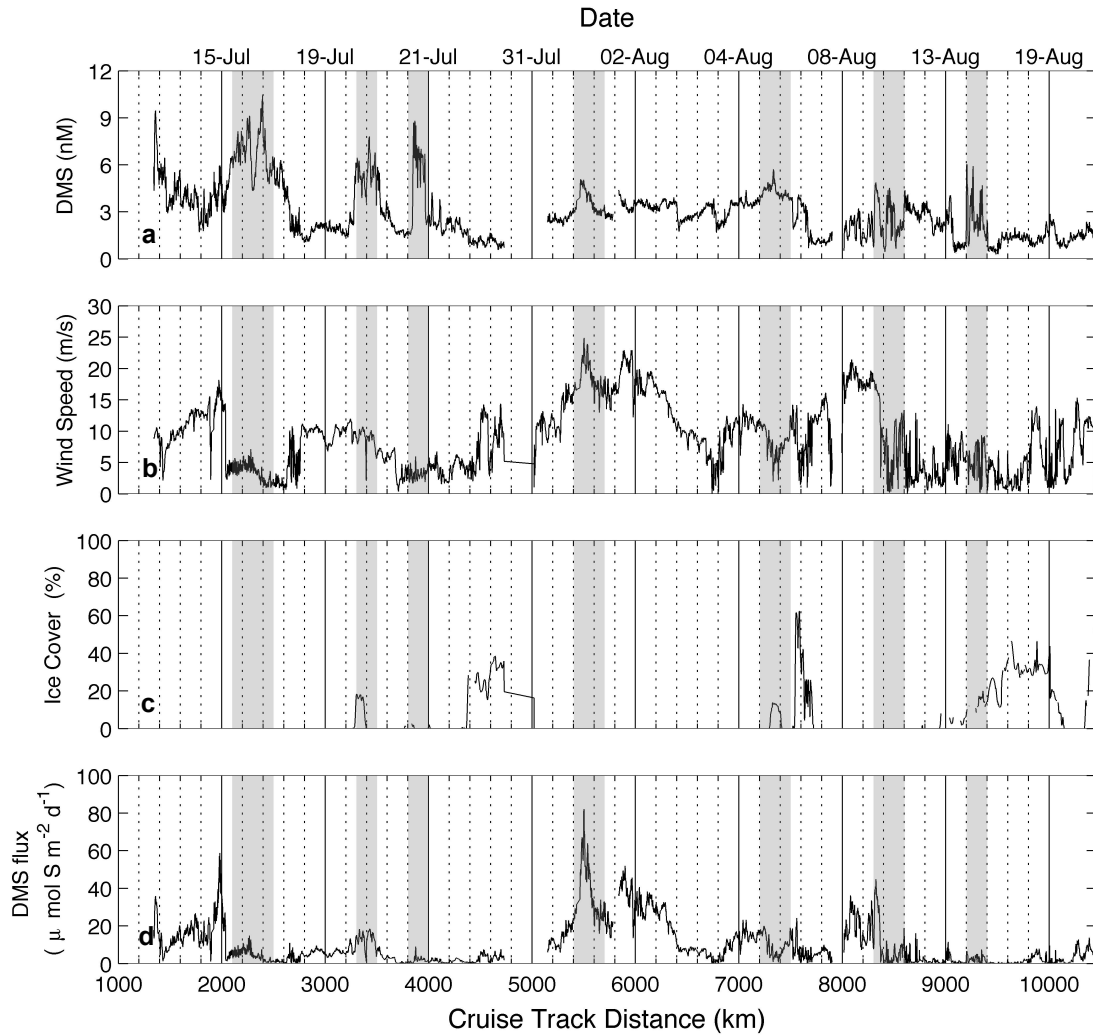


Figure 3.6. Cruise Track Record of Seawater DMS, Wind Speed, Ice Cover and DMS Flux

Areas of high DMS concentration are shaded grey, for comparison with other hydrographic features.

Chapter 4: Conclusion

This thesis aimed to further the understanding of the distribution of reduced sulphur in polar marine waters, and to help elucidate potential correlations between reduced sulphur distributions and other hydrographic variables, in order to better understand how these compounds affect changing polar ecosystems. In Chapter 2, I use high-resolution DMS measurements made in previous years by the Tortell group to revise a climatology of summertime DMS concentrations and fluxes in the Southern Ocean. In Chapter 3, I present DMS/P measurements acquired during the 2015 GEOTRACES expedition, as well as correlations with other hydrographic variables. Together, the two papers presented help to fill out existing knowledge of the reduced sulphur cycle in polar regions, while providing a baseline for future studies.

4.1 Major findings and contributions

In Chapter 2, high resolution DMS data (~700 000 measurements) made by MIMS in the Southern Ocean are added to the existing summertime PMEL dataset to create an updated Southern Ocean climatology of summertime (Dec.-Feb.) DMS concentrations and sea-air fluxes. Compared to the original climatology, the new scheme finds increased DMS concentrations and sea-air fluxes south of the Polar Frontal zone (between 60-70 °S), and increased sea-air fluxes in mid-latitude waters (40-50°S). These changes are attributable to both the inclusion of new data and the use of region-specific parameters (e.g. data cut-off thresholds and interpolation radius) in the objective analysis. DMS concentrations in the Southern Ocean exhibit weak, though statistically significant, correlations with several oceanographic variables, including ice cover, mixed-layer depth and chlorophyll-a, but no apparent relationship with satellite-derived

measures of phytoplankton photophysiology or taxonomic group abundance. This analysis highlights the importance of using regional parameters in constructing climatological DMS fields, and identifies regions where additional observations are most needed.

In Chapter 3, I present seawater concentrations of dimethylsulfide (DMS) and dimethylsulfoniopropionate (DMSP) measured across a transect from the Labrador Sea to the Western Nunavut region of the Canadian Archipelago. Using high-resolution MIMS measurements, I document strong DMS concentration gradients across surface hydrographic frontal features, highlighting the potential utility of high-resolution sampling in observing DMS dynamics across frontal structures. I find only weak relationships between DMS/P, chl *a* fluorescence, and other measured variables, including weak positive relationships between DMSP:chl *a* ratios and CHEMTAX-derived diatom, dinoflagellate, and c-3 flagellate estimates, as well as elevated DMS/P in partially ice-covered areas. These weak statistical relationships corroborate previous studies showing poor predictive power for DMS concentrations over broad spatial scales. These observations represent a significant contribution to the global Arctic DMS/O/P dataset, and can serve to provide a baseline for future measurements in the region.

4.2 Future Directions

The data contained in this thesis add considerably to the sparse observations of reduced sulphur compounds in the polar regions, using two high-resolution underway sampling instruments. Due to the very low number of observations made in these regions, future studies could significantly contribute to this work simply by expanding the spatial coverage of available data. Additionally, a better understanding of the non-*Phaeocystis* phytoplankton assemblages

associated with high DMS production in polar regions, as well as of their physiological state, would help clarify marine reduced sulphur cycling under these conditions.

From a methodological point of view, it is possible that the analysis time of the OSSCAR instrument, which has only undertaken five cruises to date, may be improved to allow for better sampling resolution, and that the temperature control of the instrument may be improved to limit instrument drift. Finally, the strong cohesion between DMS gradients and changes in other oceanographic variables that was observable by MIMS in near-real time on the Arctic cruise (Chapter 3) may be further explored, potentially leading to a better understanding of DMS dynamics across frontal structures. Future work in this field will enable researchers to better represent key processes in the sulphur cycle, and to predict potential DMS climate feedbacks.

Bibliography

- [1] A. Lana, T. G. Bell, R. Simó, S. M. Vallina, J. Ballabrera-Poy, A. J. Kettle, J. Dachs, L. Bopp, E. S. Saltzman, J. Stefels, J. E. Johnson, P. S. Liss, An updated climatology of surface dimethylsulfide concentrations and emission fluxes in the global ocean. *Global Biogeochem. Cycles* 2011, 25, GB1004. doi:10.1029/2010GB003850
- [2] R. Simó, J. Dachs, Global ocean emission of dimethylsulfide predicted from biogeophysical data. *Global Biogeochem. Cycles* 2002, 16, 1078 doi: 10.1029/2001GB001829
- [3] A. Kettle, *et al.* A global database of sea surface dimethylsulfide (DMS) measurements and a procedure to predict sea surface DMS as a function of latitude, longitude, and month. *Global Biogeochem. Cycles* 1999, 13, 299. doi: 10.1029/1999GB900004
- [4] R. Charlson, J. Lovelock, M. Andreae, S. Warren, Oceanic phytoplankton, atmospheric sulfur, cloud albedo and climate. *Nature* 1987, 326, 655. doi:10.1038/326655A0
- [5] R. Simó, S.D. Archer, C. Pedros-Alio, L. Gilpin, C.E. Stelfox-Widdicombe, Coupled dynamics of dimethylsulfoniopropionate and dimethylsulfide cycling and the microbial food web in surface waters of the North Atlantic. *Limnology and Oceanography*, 2002, 47, 53. doi: 10.4319/lo.2002.47.1.0053
- [6] M. Keller. Dimethyl sulfide production and marine phytoplankton: the importance of species composition and cell size. *Biological Oceanography* 1989, 6, 375. doi: 10.1080/01965581.1988.10749540

- [7] W. Sunda, D. J. Kieber, R. P. Kiene, S. Huntsman, An antioxidant function for DMSP and DMS in marine algae. *Nature* 2002, 418, 317. doi:10.1038/NATURE00851
- [8] M. Zubkov, B. Fuchs, S. Archer, R. Kiene, R Amann, P Burkill. Linking the composition of bacterioplankton to rapid turnover of dissolved dimethylsulphonioacetate in an algal bloom in the North Sea. *Environmental Microbiology* 2001, 3, 304. doi: 10.1046/j.1462-2920.2001.00196.x
- [9] A. Hatton, G. Malin, S.M. Turner, P.S. Liss. DMSO - A Significant Compound in the Biogeochemical Cycle of DMS. *Biological and Environmental Chemistry of DMSP and Related Sulfonium Compounds* 1996, 405. doi: 10.1007/978-1-4613-0377-0_35
- [10] J. Stefels, M. Steinke, S. Turner, G. Malin, and S. Belviso, *Environmental constraints on the production and removal of the climatically active gas dimethylsulphide (DMS) and implications for ecosystem modeling. Biogeochemistry* 2007, 83, 245. doi: 10.1007/s10533-007-9091-5
- [11] D.C. Yoch, *Dimethylsulfoniopropionate: Its Sources, Role in the Marine Food Web, and Biological Degradation to Dimethylsulfide. Applied and Environmental Microbiology*, 2002, 68, 5804. doi: 10.1128/AEM.68.12.5804-5815.2002
- [12] P. K. Quinn, T. S. Bates, *The case against climate regulation via oceanic phytoplankton sulphur emissions. Nature* 2011, 480, 51. doi:10.1038/NATURE10580
- [13] G.P. Ayers, J.L. Gras, *Seasonal relationship between cloud condensation nuclei and aerosol methanesulphonate in marine air. Nature* 1991, 353, 834. doi:10.1038/353834a0

- [14] O Rempillo, AM Seguin, AL Norman, Dimethyl sulfide air-sea fluxes and biogenic sulfur as a source of new aerosols in the Arctic fall. *Journal of Geophysical Research* (2011). 116, 1984. doi: 10.1029/2011JD016336
- [15] R. Simo', Production of atmospheric sulfur by oceanic plankton: biogeochemical, ecological and evolutionary links. *Trends Ecol. Evol.* 2001, 16, 287. doi:10.1016/S0169-5347(01)02152-8
- [16] O. Boucher, C. Moulin, S. Belviso, O. Aumont, L. Bopp, E. Cosme, R. von Kuhlmann, M. G. Lawrence, M. Pham, M. S. Reddy, J. Sciare, C. Venkataraman, DMS atmospheric concentrations and sulphate aerosol indirect radiative forcing: a sensitivity study to the DMS source representation and oxidation. *Atmos. Chem. Phys.* 2003, 3, 49. doi:10.5194/ACP-3-49-2003
- [17] M. A. Thomas, P. Suntharalingam, L. Pozzoli, S. Rast, A. Devasthale, S. Kloster, J. Feichter, T. M. Lenton, Quantification of DMS aerosol–cloud–climate interactions using the ECHAM5-HAMMOZ model in a current climate scenario. *Atmos. Chem. Phys.* 2010, 10, 7425. doi:10.5194/ACP-10-7425-2010
- [18] J. Stefels, Physiological aspects of the production and conversion of DMSP in marine algae and higher plants. *J. Sea Res.* 2000, 43, 183. doi:10.1016/S1385-1101(00)00030-7
- [19] A. J. Gabric, B. Qu, P. Matrai, A. Hirst, Modeling estimates of the global emission of dimethylsulfide under enhanced greenhouse conditions. *Global Biogeochem. Cycles* 2004, 18, GB2014.
- [20] A. F. Vezina, Ecosystem modelling of the cycling of marine dimethylsulfide: a review of current approaches and of the potential for extrapolation to global scales. *Can.*

- J. Fish. Aquat. Sci. 2004, 61, 845. doi:10.1139/F04-025
- [21] P. Cameron-Smith, S. Elliott, M. Maltrud, D. Erickson, O. Wingenter, Changes in dimethyl sulfide oceanic distribution due to climate change. *Geophys. Res. Lett.* 2011, 38, L07704. doi:10.1029/2011GL047069
- [22] V. Schoemann, S. Becquevort, J. Stefels, V. Rousseau, C. Lancelot, Phaeocystis blooms in the global ocean and their controlling mechanisms: a review. *J. Sea Res.* 2005, 53, 43. doi:10.1016/J.SEARES.2004.01.008
- [23] P. Boyd, P. J. Harrison, Phytoplankton dynamics in the NE Subarctic 50 Pacific. *Deep Sea Res. Part II Top. Stud. Oceanogr.* 1999, 46, 2405. doi:10.1016/S0967-0645(99)00069-7
- [24] P. W. Boyd, Environmental factors controlling phytoplankton processes in the Southern Ocean. *J. Phycol.* 2002, 38, 844. doi:10.1046/J.1529-8817.2002.T01-1-01203.X
- [25] D. Lubin, J. Frederick, C. Rocky Booth, T. Lucas, D. Neuschuler, Measurements of enhanced springtime ultraviolet radiation at Palmer Station, Antarctica. *Geophys. Res. Lett.* 1989, 16, 783. doi:10.1029/GL016I008P00783
- [26] K. R. Arrigo, K. Lowry, G. van Dijken, Dynamics of sea ice and phytoplankton in polynyas of the Amundsen Sea, Antarctica. *Deep Sea Res. Part II Top. Stud. Oceanogr.* 2012, 71, 5. doi:10.1016/J.DSR2.2012.03.006
- [27] P. D. Tortell, Dissolved gas measurements in oceanic waters made by membrane inlet mass spectrometry. *Limnol. Oceanogr. Methods* 2005, 3, 24.
- [28] E. S. Saltzman, W. J. De Bruyn, M. J. Lawler, C. A. Marandino, C. A. McCormick, A chemical ionization mass spectrometer for continuous underway shipboard analysis of

dimethylsulfide in near-surface seawater. *Ocean Science* 2009, 5, 537. doi:10.5194/OS-5-537-2009

[29] P. D. Tortell, C. Guégen, M. C. Long, C. D. Payne, P. Lee, G. R. DiTullio, Spatial variability and temporal dynamics of surface water pCO₂, DO₂/Ar and dimethylsulfide in the Ross Sea, Antarctica. *Deep Sea Res. Part I Oceanogr. Res. Pap.* 2011, 58, 241. doi:10.1016/J.DSR.2010.12.006

[30] P. D. Tortell, M. C. Long, C. D. Payne, A.-C. Alderkamp, P. Dutrieux, K. Arrigo, Spatial distribution of pCO₂, DO₂/Ar and dimethylsulfide (DMS) in polynya waters and the sea-ice zone of the Amundsen Sea, Antarctica. *Deep Sea Res. Part II Top. Stud. Oceanogr.* 2011, 71, 77.

[31] P. D. Tortell, M. C. Long, Spatial and temporal variability of biogenic gases during the Southern Ocean spring bloom. *Geophys. Res. Lett.* 2009, 36, L01603. doi:10.1029/2008GL035819

[32] E. C. Asher, J. W. H. Dacey, T. Jarníková, P. D. Tortell, Measurement of DMS, DMSO, and DMSP in natural waters by automated sequential chemical analysis. *Limnol. Oceanogr. Methods* 2015, 36, L01603.

[33] R. Johnson, P. G. Strutton, S. W. Wright, A. McMinn, K.M. Meiners, Three improved satellite chlorophyll algorithms for the Southern Ocean. *J. Geophys. Res. – Oceans* 2013, 118, 3694. doi:10.1002/JGRC.20270

[34] C. de Boyer Montegut, G. Madec, A. S. Fischer, A. Lazar, D. Iudicone, Mixed-layer depth over the global ocean: an examination of profile data and a profile-based climatology. *J. Geophys. Res. – Oceans* AQ3 2004, 109, C12003. doi:10.1029/2004JC002378

- [35] R. P. Kiene, D. Slezak, Low dissolved DMSP concentrations in seawater revealed by small-volume gravity filtration and dialysis sampling. *Limnol. Oceanogr. Methods* 2006, 4, 80. doi:10.4319/LOM.2006.4.80
- [36] J. Stefels, L. Dijkhuizen, Characteristics of DMSP lyase in *Phaeocystis* sp. (Prymnesiophyceae). *Mar. Ecol. Prog. Ser.* 1996, 131, 307. doi:10.3354/MEPS131307
- [37] G. R. DiTullio, W. O. Smith, Spatial patterns in phytoplankton biomass and pigment distributions in the Ross Sea. *J. Geophys. Res. – Oceans* 1996, 101(C8), 18 467. doi:10.1029/96JC00034
- [38] A. R. Longhurst, *Ecological Geography of the Sea* 2007 (Elsevier Inc.: London).
- [39] International Hydrographic Bureau, *Limits of Seas and Oceans. Special Publication 23* 1987 (International Hydrographic Bureau: Monaco).
- [40] S. L. Barnes, A technique for maximizing details in numerical weather map analysis. *J. Appl. Meteorol.* 1964, 3, 396. doi:10.1175/1520-0450
- [41] R. A. Locarnini, A. Mishonov, J. Antonov, T. P. Boyer, H. E. Garcia, O. K. Baranova, M. M. Zweng, D. R. Johnson, *World Ocean Atlas 2009, Vol. 1. Temperature 2009* (Ocean Climate Laboratory: Silver Spring, MD).
- [42] P. D. Nightingale, G. Malin, C. S. Law, A. J. Watson, P. S. Liss, M. I. Liddicoat, J. Boutin, R. C. Upstill-Goddard, In situ evaluation of air–sea gas exchange parameterizations using novel conservative and volatile tracers. *Global Biogeochem. Cycles* 2000, 14, 373. doi:10.1029/1999GB900091
- [43] E. S. Saltzman, D. B. King, K. Holmen, C. Leck, Experimental determination of the diffusion coefficient of dimethylsulfide in water. *J. Geophys. Res.* 1993, 98, 16 481. doi:10.1029/93JC01858

- [44] B. Loose, W. R. McGillis, P. Schlosser, D. Perovich, T. Takahashi, Effects of freezing, growth, and ice cover on gas transport processes in laboratory seawater experiments. *Geophys. Res. Lett.* 2009, 36, L05603. doi:10.1029/2008GL036318
- [45] M. J. Behrenfeld, T. K. Westberry, E. S. Boss, R. T. O'Malley, D.A. Siegel, J.D.Wiggert, B.A. Franz, C.R.McClain,G. C. Feldman, S. C. Doney, J. K. Moore, G. Dall'Olmo, A. J. Milligan, I. Lima, N. Mahowald, Satellite-detected fluorescence reveals global physiology of ocean phytoplankton. *Biogeosciences* 2009, 6, 779.
doi:10.5194/BG-6-779-2009
- [46] Y. Huot, B. A. Franz, M. Fradette, Estimating variability in the quantum yield of sun-induced chlorophyll fluorescence: a global analysis of oceanic waters. *Remote Sens. Environ.* 2013, 132, 238. doi:10.1016/J.RSE.2013.01.003
- [47] T. J. Browning, H. A. Bouman, C. M. Moore, Satellite-detected fluorescence: decoupling non-photochemical quenching from iron stress signals in the South Atlantic and Southern Ocean. *Global Biogeochem. Cycles* 2014, 28, 510.
doi:10.1002/2013GB004773
- [48] Z. Ben Mustapha, S. Alvain, C. Jamet, H. Loisel, D. Dessailly, Automatic classification of water-leaving radiance anomalies from global SeaWiFS imagery: application to the detection of phytoplankton groups in open oceanwaters. *Remote Sens. Environ.* 2014, 146, 97. doi:10.1016/J.RSE.2013.08.046
- [49] S. M. Vallina, R. Simo, Strong relationship between DMS and the solar radiation dose over the global surface ocean. *Science* 2007, 315, 506.
doi:10.1126/SCIENCE.1133680
- [50] A. Morel, Optical modeling of the upper ocean in relation to its biogenous matter

content (case I waters). *J. Geophys. Res. – Oceans* 1988, 93, 10 749.

doi:10.1029/JC093IC09P10749

[51] E. C. Asher, A. Merzouk, P. D. Tortell, Fine-scale spatial and temporal variability of surface water dimethylsulfide (DMS) concentrations and sea–air fluxes in the NE

Subarctic Pacific. *Mar. Chem.* 2011, 126,63. doi:10.1016/J.MARCHEM.2011.03.009

[52] A. S. Mahajan, S. Madnavis, M. A. Thomas, L. Pozzoli, S. Gupta, S.-J. Royer, A.

Saiz-Lopez, R. Simo, Quantifying the impacts of an updated global dimethyl sulfide climatology on cloud microphysics and aerosol radiative forcing. *J. Geophys. Res.–*

Atmos. 2015, 120, 2524. doi:10.1002/2014JD022687

[53] S. Preunkert, M. Legrand, B. Jourdain, C. Moulin, S. Belviso, N. Kasamatsu, M.

Fukuchi, T. Hirawake, Interannual variability of dimethylsulfide in air and seawater and its atmospheric oxidation byproducts (methanesulfonate and sulfate) at Dumont

d’Urville, coastal Antarctica (1999–2003). *J. Geophys. Res. – Atmos.* 2007, 112(D6),

D06306. doi:10.1029/2006JD007585

[54] R. H. Rhodes, N. A. N. Bertler, J. A. Baker, S. B. Sneed, H. Oertner, K. R. Arrigo,

Sea ice variability and primary productivity in the Ross Sea, Antarctica, from

methylsulphonate snow record. *Geophys. Res. Lett.* 2009, 36, L10704.

[55] H. J. Zemmeling, L. Houghton, J. W. H. Dacey, A. P. Worby, P. S. Liss, Emission of dimethylsulfide from Weddell Sea leads. *Geophys. Res. Lett.* 2005, 32, L23610.

doi:10.1029/2005GL024242

[56] R. Simo´ , J. Dachs, Global ocean emission of dimethylsulfide predicted from biogeophysical data. *Global Biogeochem. Cycles* 2002, 16, 1078.

doi:10.1029/2001GB001829 AQ4

- [57] G. R. DiTullio, W. O. Smith, Relationship between dimethylsulfide and phytoplankton pigment concentrations in the Ross Sea, Antarctica. *Deep Sea Res. Part I Oceanogr. Res. Pap.* 1995, 42, 873. doi:10.1016/0967-0637(95)00051-7
- [58] L. Bopp, O. Boucher, O. Aumont, S. Belviso, J.-L. Dufresne, M. Pham, P. Monfray, Will marine dimethylsulfide emissions amplify or alleviate global warming? A model study. *Can. J. Fish. Aquat. Sci.* 2004, 61, 826. doi:10.1139/F04-045
- [59] G. M. Fragoso, W. O. Smith, Influence of hydrography on phytoplankton distribution in the Amundsen and Ross Seas, Antarctica. *J. Mar. Syst.* 2012, 89, 19. doi:10.1016/J.JMARSYS.2011.07.008
- [60] A.-C. Alderkamp, G. L. van Dijken, K. E. Lowry, T. L. Connelly, M. Lagerstrom, R. M. Sherrell, C. Haskins, E. Rogalsky, O. Schofield, S. E. Stammerjohn, P. L. Yager, K. R. Arrigo, Fe availability drives phytoplankton photosynthesis rates during spring bloom in the Amundsen Sea Polynya, Antarctica. *Elementa* 2015, 3, 43. doi:10.12952/JOURNAL.ELEMENTA.000043
- [61] A.-C. Alderkamp, M. M. Mills, G. L. van Dijken, P. Laan, C.-E. Thuroczy, L. J. A. Gerringa, H. J. W. de Baar, C. D. Payne, R. J. W. Visser, A. G. J. Buma, K. R. Arrigo, Iron from melting glaciers fuels phytoplankton blooms in the Amundsen Sea (Southern Ocean): phytoplankton characteristics and productivity. *Deep Sea Res. Part II Top. Stud. Oceanogr.* 2012, 71, 32. doi:10.1016/J.DSR2.2012.03.005
- [62] K. R. Arrigo, G. L. van Dijken, Phytoplankton dynamics within 37 Antarctic coastal polynya systems. *J. Geophys. Res. – Oceans* 2003, 108(C8), 3271. doi:10.1029/2002JC001739
- [63] R. K. Laubscher, R. Perissinotto, C. D. McQuaid, Phytoplankton production and

biomass at frontal zones in the Atlantic sector of the Southern Ocean. *Polar Biol.* 1993, 13, 471. doi:10.1007/BF00233138

[64] S. Sokolov, Chlorophyll blooms in the Antarctic Zone south of Australia and New Zealand in reference to the Antarctic Circumpolar Current fronts and sea ice forcing. *J. Geophys. Res. –Oceans* 2008, 113, C03022.

[65] R. P. Kiene, D. J. Kieber, D. Slezak, D. A. Toole, D. A. del Valle, J. Bisgrove, J. Brinkley, A. Rellinger, Distribution and cycling of dimethylsulfide, dimethylsulfoniopropionate, and dimethylsulfoxide during spring and early summer in the Southern Ocean south of New Zealand. *Aquat. Sci.* 2007, 69, 305. doi:10.1007/S00027-007-0892-3

[66] T. Takahashi, C. Sweeney, S. C. Sutherland, D. W. Chipman, J. Goddard, S. I. Rubin, Method of underway pCO₂ measurements in surface waters and the atmosphere during the Aesops expeditions, 1996–1998 in the Pacific Sector of the Southern Ocean and the Ross Sea 2000 (US Joint Global Ocean Flux Study Data Center, Woods Hole Oceanographic Institution: Woods Hole, MA).

[67] G. Malin, W.H. Wilson, G. Bratbak, P.S. Liss, N.H. Mann. Elevated production of dimethylsulfide resulting from viral infection of cultures of *Phaeocystis pouchetii*. *Limnology and Oceanography* 1998, 43, 1389. doi: 10.4319/lo.1998.43.6.1389

[68] R. Kiene, L. Linn, S. Archer. New and important roles for DMSP in marine microbial communities. *Journal of Sea Research* 2000, 43, 209. doi:10.1016/S1385-1101(00)00023-X

- [69] M. Woodhouse, K. Carslaw, G. Mann, S. Vallina, M. Vogt, P. Halloran, O. Boucher. Low sensitivity of cloud condensation nuclei to changes in the sea-air flux of dimethylsulphide. *Atmos Chem Phys* 2010, 10, 7545. doi:10.5194/acp-10-7545-2010
- [70] R. Chang, S.J. Sjostedt, J.R. Pierce. Relating atmospheric and oceanic DMS levels to particle nucleation events in the Canadian Arctic. *Journal of Geophysical Research*. 2011, 116, DOOS03. doi: 10.1029/2011JD015926
- [71] K.R. Arrigo, D.K. Perovich, R.S. Pickart, Z.W. Brown, et al. Massive phytoplankton blooms under Arctic sea ice. *Science* 2012, 336, 1408. doi: 10.1126/science.1215065
- [72] K.R. Arrigo, G. van Dijken, S. Pabi. Impact of a shrinking Arctic ice cover on marine primary production. *Geophysical Research Letters* 2008, 35, L19603. doi: 10.1029/2008GL035028
- [73] M. Levasseur. Impact of Arctic meltdown on the microbial cycling of sulphur. *Nat Geoscience* 2013, 6, 691. doi:10.1038/ngeo1910
- [74] J. Dacey, N. Blough. Hydroxide decomposition of dimethylsulfoniopropionate to form dimethylsulfide. *Geophysical Research Letters* 1987, 14, 1246. doi: 10.1029/GL014i012p01246
- [75] N.A. Welschmeyer. Fluorometric analysis of chlorophyll a in the presence of chlorophyll b and pheopigments. *Limnology and Oceanography* 1994, 39, 1985. doi: 10.4319/lo.1994.39.8.198
- [76] Pinckney J, Papa R, Zingmark R. Comparison of high-performance liquid chromatographic, spectrophotometric, and fluorometric methods for determining chlorophyll *a* concentrations in estuarine sediments. *Journal of Microbiological Methods*. 1994; 19(1):59-66. doi:10.1016/0167-7012(94)90026-4

- [77] P. Coupel , A. Matsuoka, D. Ruiz-Pino, M. Gosselin, D. Marie, J.-É. Tremblay , M. Babin. Pigment signatures of phytoplankton communities in the Beaufort Sea. *Biogeosciences* 2015, 12, 991. doi:10.5194/bg-12-991-2015
- [78] R. Taylor, D. Semeniuk, C. Payne, J. Zhou, J-E. Tremblay, J. Cullen, M. Maldonado, Colimitation by light, nitrate, and iron in the Beaufort Sea in late summer. *Journal of Geophysical Research: Oceans* 2013, 118, 3260. doi:10.1002/jgrc.20244.
- [79] M. Levasseur, M. Gosselin, S. Michaud. A new source of dimethylsulfide (DMS) for the arctic atmosphere: ice diatoms. *Marine Biology* 1994, 121, 381. doi: 10.1007/BF00346748
- [80] R.C. Bouillon, P. Lee, S. de Mora, M. Levasseur, C. Lovejoy. Vernal distribution of dimethylsulphide, dimethylsulphonioacetate, and dimethylsulphoxide in the North Water in 1998. *Deep Sea Research II* 2002, 49, 5171. doi:10.1016/S0967-0645(02)00184-4
- [81] J. Motard-Côté, M. Levasseur, M. G. Scarratt, S. Michaud, Y. Gratton, R. B. Rivkin, K. Keats, M. Gosselin, J.-É. Tremblay, R. P. Kiene, C. Lovejoy. Distribution and metabolism of dimethylsulfonylacetate (DMSP) and phylogenetic affiliation of DMSP-assimilating bacteria in northern Baffin Bay/Lancaster Sound. *Journal of Geophysical Research* 2011, 117, C00G11. doi:10.1029/2011JC007330, 2012
- [82] M. Luce, M. Levasseur, M. G. Scarratt, S. Michaud, S.-J. Royer, R. Kiene, C. Lovejoy, M. Gosselin, M. Poulin, Y. Gratton, M. Lizotte. Distribution and microbial metabolism of dimethylsulfonylacetate

and dimethylsulfide during the 2007 Arctic ice minimum. *Journal of Geophysical Research* 2011, 116, C00G07. doi:10.1029/2010JC006914

[83] M. Gali, R. Simo. Occurrence and cycling of dimethylated sulfur compounds in the Arctic during summer receding of the ice edge. *Marine Chemistry* 2010, 122, 105. doi:10.1016/j.marchem.2010.07.003

[84] R. Simo, C. Pedros-Alio. Role of vertical mixing in controlling the oceanic production of dimethyl sulphide. *Nature* 1999, 402, 396.

[85] C. Leck, C. Persson. The central Arctic Ocean as a source of dimethylsulfide – Seasonal variability in relation to biological activity. *Tellus* 1996, 48, 157. DOI: 10.1034/j.1600-0889.1996.t01-1-00003.x

[86] J.-É. Tremblay, S. Bélanger, D. G. Barber, M. Asplin, J. Martin, G. Darnis, L. Fortier, Y. Gratton, H. Link, P. Archambault, A. Sallon, C. Michel, W. J. Williams, B. Philippe, M. Gosselin. Climate forcing multiplies biological productivity in the coastal Arctic Ocean. *Geophysical Research Letters* 2011, 38, L18604. doi:10.1029/2011GL048825

[87] P. Matrai, M. Vernet. Dynamics of the vernal bloom in the marginal ice zone of the Barents Sea: Dimethyl sulfide and dimethylsulfoniopropionate budgets. *Journal of Geophysical Research* 1997, 102, 965. doi: 10.1029/96jc03870

[88] M. Levasseur, Impact of Arctic meltdown on the microbial cycling of sulphur. *Nature Geoscience* 2013, 6, 691. doi: 10.1038/NGEO1910